Cell Reports

Article

A highland-adaptation mutation of the Epas1 protein increases its stability and disrupts the circadian clock in the plateau pika

Graphical abstract

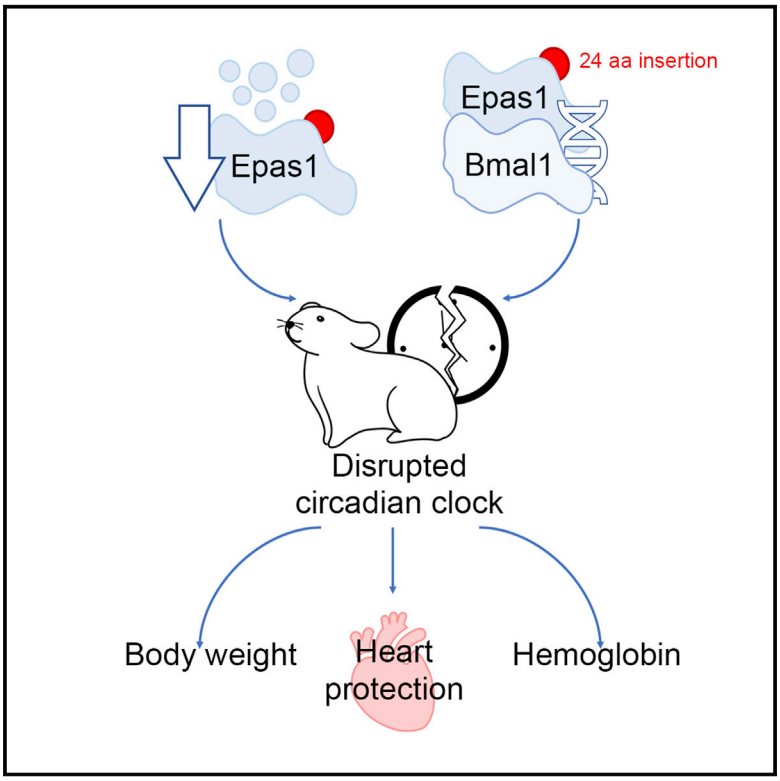

Highlights

- The plateau pika circadian clock is disrupted, yet individual clock genes are functional
- Multiple *Epas1* splice variants explain the observed difference in pika rhythmicity
- Epas1 dimerizes with Bmal1 and disrupts the intracellular clockwork
- Ectopic expression of plateau pika *Epas1* in SCN recapitulates the arrhythmicity

Authors

Na Liu, Hongni Tian, Ziqing Yu, ..., Yanming Zhang, Tao Cai, Eric Erquan Zhang

Correspondence

zhangym@nwipb.cas.cn (Y.Z.), caitao@nibs.ac.cn (T.C.), zhangerquan@nibs.ac.cn (E.E.Z.)

In brief

Liu et al. identify a mutation at the 5′ juncture of Intron14 of *Epas1* in the plateau pika, which results in a 24-residue insertion that stabilizes the Epas1 protein. Epas1 interacts with the core-clock component Bmal1 and disrupts the circadian rhythm of the plateau pika, which confers benefits for highland adaptation.

Liu et al., 2022, Cell Reports *39*, 110816
May 17, 2022
https://doi.org/10.1016/j.celrep.2022.110816

CellPress

Cell Reports

CellPress
OPEN ACCESS

Article

A highland-adaptation mutation of the Epas1 protein increases its stability and disrupts the circadian clock in the plateau pika

Na Liu,[1,2,3,14] Hongni Tian,[1,2,4,5,14] Ziqing Yu,[2,6,14] Haijiao Zhao,[1,2,14] Wenjing Li,[7,14] Di Sang,[2,6] Keteng Lin,[2] Yilin Cui,[2,8] Meimei Liao,[2] Zhancong Xu,[2,6] Chen Chen,[2] Ying Guo,[2] Yibing Wang,[2] Huan-wei Huang,[2] Jiawen Wang,[2] He Zhang,[7,9] Wei Wu,[10] He Huang,[4] Shengqing Lv,[5] Zhenqian Guo,[11] Wei Wang,[2] Sanduo Zheng,[2] Fengchao Wang,[2] Yanming Zhang,[7,12,*] Tao Cai,[2,*] and Eric Erquan Zhang[2,6,13,15,*]

[1]College of Life Sciences, Beijing Normal University, Beijing 100875, China
[2]National Institute of Biological Sciences, Beijing 102206, China
[3]Hubei Engineering Research Center of Special Wild Vegetables Breeding and Comprehensive Utilization Technology, Hubei Key Laboratory of Edible Wild Plants Conservation and Utilization, School of Life Sciences, Hubei Normal University, Huangshi, Hubei Province 435002, China
[4]Department of Anesthesiology, The Second Affiliated Hospital of Chongqing Medical University, Chongqing 400010, China
[5]Department of Neurosurgery, Xinqiao Hospital, Chongqing 400038, China
[6]Graduate School of Peking Union Medical College & Chinese Academy of Medical Sciences, Beijing 100006, China
[7]Key Laboratory of Adaptation and Evolution of Plateau Biota, Northwest Institute of Plateau Biology, Chinese Academy of Sciences, Xining, Qinghai Province 810008, China
[8]Neuroscience Program, Smith College, Northampton, MA 01063, USA
[9]Department of Pathology, Henan Cancer Hospital, Zhengzhou, Henan Province 450008, China
[10]Department of Neurology, The Second Affiliated Hospital of Nanchang University Medical School, Nanchang, Jiangxi Province 330006, China
[11]Shuimu BioSciences Ltd., Beijing 102206, China
[12]Qinghai Provincial Key Laboratory of Animal Ecological Genomics, Xining, Qinghai Province 810008, China
[13]Tsinghua Institute of Multidisciplinary Biomedical Research, Tsinghua University, Beijing 102206, China
[14]These authors contributed equally
[15]Lead contact
*Correspondence: zhangym@nwipb.cas.cn (Y.Z.), caitao@nibs.ac.cn (T.C.), zhangerquan@nibs.ac.cn (E.E.Z.)
https://doi.org/10.1016/j.celrep.2022.110816

SUMMARY

The Qinghai-Tibet Plateau (QTP) harbors hundreds of species well adapted to its extreme conditions, including its low-oxygen (hypoxic) atmosphere. Here, we show that the plateau pika—a keystone mammal of the QTP—lacks robust circadian rhythms. The major form of the plateau pika Epas1 protein includes a 24-residue insert caused by a point mutation at the 5′ juncture site of Intron14 and is more stable than other mammalian orthologs. Biochemical studies reveal that an Epas1-Bmal1 complex with lower *trans*-activation activity occupies the E1/E2 motifs at the promoter of the core-clock gene *Per2*, thus explaining how an *Epas1* mutation—selected in the hypoxic conditions of the QTP—disrupts the molecular clockwork. Importantly, experiments with hypoxic chambers show that mice expressing the plateau pika *Epas1* ortholog in their suprachiasmatic nucleus have dysregulated central clocks, and pika *Epas1* knockin mice reared in hypoxic conditions exhibit dramatically reduced heart damage compared with wild-type animals.

INTRODUCTION

The circadian clock widely exists in most terrestrial organisms (Dunlap, 1999; Zhang and Kay, 2010). Recently, a comparative genomics study of the Arctic reindeer attempted to decipher how the mammalian clock is affected in the North Pole (Lin et al., 2019), where the months-long constant light or darkness of each year has been proposed to impact its internal clockwork for more than a decade (van Oort et al., 2005). Besides extreme latitudes, it may be possible for the behavior of cellular clockwork to be altered in other extreme environmental contexts, for example, in the "third pole" of the world: the Qinghai-Tibet Plateau (QTP), an area with notable hypoxic conditions.

The QTP has been on the rise since approximately 50 million years ago (Mya), generating an average elevation exceeding 4,500 m of highland home to hundreds of species adapted to the extreme conditions, including but not limited to low oxygen, low temperature, and drastic daily weather changes (Plummer et al., 2016; Royden et al., 2008). The genus *Ochotona* (pika, or mousehare) emerged around the beginning of the QTP rise and was concentrated in the area of Central-East Asia (Figure S1) (Rose et al., 2008; Smith et al., 2010). The pika is a family within

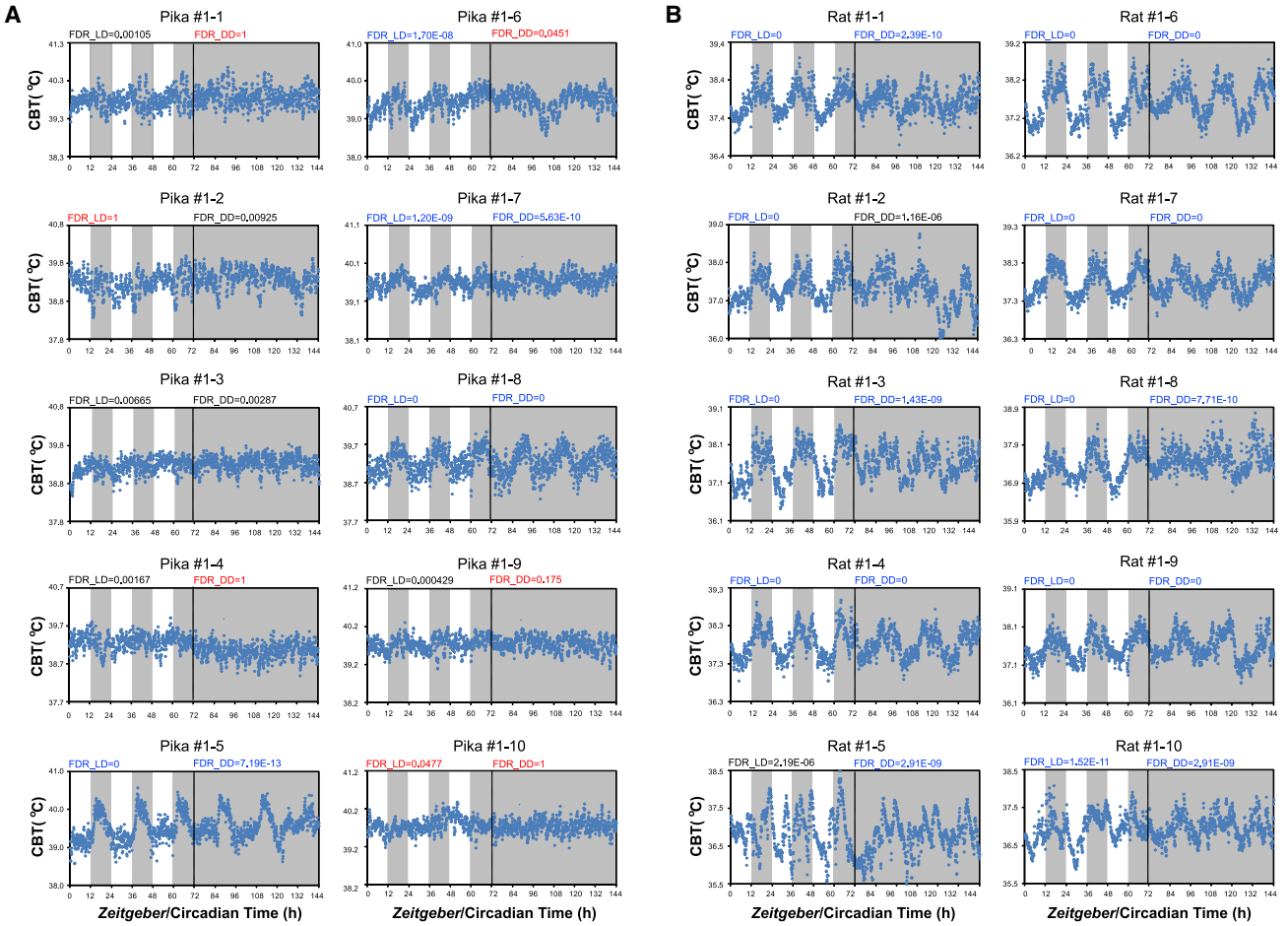

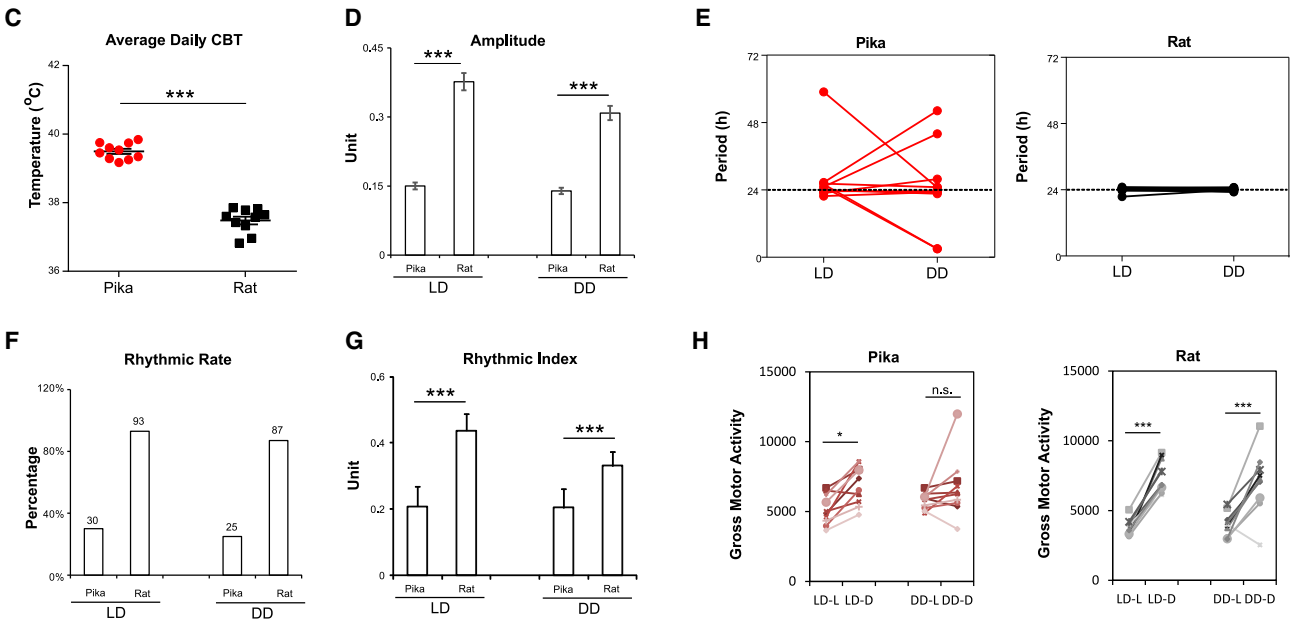

(legend on next page)

the order *Lagomorphs*, including the *Leporidae* (rabbits and hares). Pika partially resemble their relatives (rabbits), with short limbs, round bodies, an even fur coat, and no external tail. At the same time, they are generally smaller than rabbits and have short, round ears (Figure S1, bottom left insert).

The fossil record shows that pika species spread across Asia (Rose et al., 2008), then westward to Europe (López Martínez, 2001), and eastward to the Nearctic Region via the Beringia over about 2–3 Mya (Lanier and Olson, 2009) (Figure S1). Approximately 28 *Ochonota* species are observed throughout Asia (Yu et al., 2000). For instance, plateau pika (Pl-Pika; *O. curzoniae*) and Pamir's pika (Afghan pika, *O. rufescens*) inhabited near their place of origin and adapted to the environment along with the geographic changes, particularly during the drastic uplift time of the QTP and Pamir plateau in the mid-late Pliocene (ca. 3–4 Mya), before which the altitude of the region was lower than 1,000 m (Plummer et al., 2016; Royden et al., 2008). Steppe pika (*O. pusilla*) and Siberian pika (*O. hyperborea*), conversely, migrated to low-/intermediate-altitude mountainous areas (Smith et al., 2010). The branch in Europe gradually evolved into *Prolagus*, an extinct pika genus consisting of several prehistoric species, and only one, Sardinian pika (*Prolagus* sardus), survived until the early 1800s (Dawson, 1969). Another branch in the Nearctic underwent a complex diversification in the region (Lanier and Olson, 2009), where Collared pika (*O. collaris*) and American pika (Am-Pika; *O. princeps*) are the only two remaining species outside of Asia (Yu et al., 2000).

Pl-Pika (or black-lipped pika) is the most populous mammal in the QTP and is a keystone animal in recycling nutrients in the soil, reducing overland flow, and preserving the ecosystem of this highland, which is located upstream from watersheds hosting more than 20% of the whole-world human population (Smith et al., 2019). Am-Pika has been sequenced for the whole genome via a "29 mammals project" (Lindblad-Toh et al., 2011). Comparing the genome of plateau pika and American pika, we might potentially find the specificity of species in the QTP.

A previous study suggested that Pamir's pika, a branch of mousehare primarily native to central Asia mountains, lost its daily core-body-temperature rhythm, with the molecular mechanism yet unknown (Luo et al., 1997). In the present study, we measured the clock machinery of Pl-Pika at behavioral, genomic, cellular, biochemical, and structural levels. We demonstrate that Pl-Pika lost its circadian rhythms both *in vivo* and *in vitro*. The molecular mechanism is due to the enhanced stability of the Epas1 protein, resulting from highland adaptation and subsequently leading to the disruption of the clock.

RESULTS

Pl-Pika population is physiologically and behaviorally arrhythmic

To investigate whether pikas possess a robust circadian rhythm in their daily activity, we utilized a telemetric transmitter system to simultaneously record core body temperatures and gross-motor activity in a laboratory located in Qinghai Province, China, where the ambient oxygen concentration is ~60% of that at sea level (Parati et al., 2018). Both physiological and behavioral monitoring and rhythmicity analysis revealed that these housed pika individuals exhibited weak or no circadian rhythms (Figures 1A and S2A). In contrast, rats bred and reared at the same high-altitude institution for more than 20 generations exhibited robust rhythmicity at physiological and behavioral levels (Figures 1B and S2B).

First, we found that the average core body tempertature of pikas was significantly higher than that of rat (Figures 1C and S2C). To vigorously assess the robustness of the whole animal rhythms, we applied two widely used algorithms of Lomb-Scargle periodogram and NLLS (which are available within R package MetaCycle and a web-based BioDare2 package). We observed that the robustness of the clock-driven physiology and behavior is significantly lower in pikas than in rats, as evaluated by the rhythmicity index (Leise, 2017), rhythmic rate based on false discovery rate (FDR), amplitude, and the period variation between light-dark (LD) and constant darkness (DD) in the circadian range (period of 20–28 h) (Liu et al., 2007) (Figures 1D–1H and S2D–S2F).

It is worth noting that similar arrhythmicity phenotypes for the pikas were observed in animals housed in both DD and 12:12 h LD photoperiod conditions, clearly suggesting that the observed phenotypes were not related to light entrainment but intrinsically embedded (genetic) rather than ectopically (epigenetic) due to the environment.

Figure 1. Plateau pika exhibits weak circadian rhythms at the physiological and behavioral levels

(A and B) Longitudinal recordings of the core body temperatures (CBTs) of individual pika (A) and rat (B) animals, suggesting that pika does not exhibit robust daily rhythms at the whole animal level. #1 represents the first batch of animals that we recorded, and the second batch (#2) data are listed in Figure S2. Animals were monitored in the lab for at least 3 days of light/dark (LD, 12:12 h) cycle, followed by 3 days of constant darkness (DD); open bars are the light phase, and gray regions indicate the dark phase. The values of false discovery rate (FDR) are listed in each subpanel; blue indicates robust rhythmicity (FDR < 10^{-6}), black indicates arguable rhythmicity (10^{-6} < FDR < 0.01), and red indicates no rhythmicity (FDR > 0.01).

(C) The average daily CBT of pika was about 1.5°C higher than that of rat.

(D–G) Analysis of circadian rhythms, including the following parameters: amplitude (D), period variation between LD and DD (E), rhythmicity rate (percentage of individuals with good rhythmicity) (F), and rhythmicity index (G). The complete analyzed data are provided in Table S1, and the detailed analysis procedure is supplemented in the STAR Methods.

(H) The behavioral rhythms of the pika were not robust: the gross-motor activity of pika was indistinguishable between subjective day and night; in contrast, rats showed a clear pattern of nocturnal activity in the same experimental conditions.

LD-L, average of light phase in LD scheme; LD-D, dark phase in LD scheme; DD-L, subjective daytime in DD condition; DD-D, subjective nighttime in DD condition. Error bars represent SEM, and statistical significance was determined using two-sided Student's t tests when only two groups were analyzed. One-way ANOVA was used when more than two groups were being analyzed. *p < 0.05, **p < 0.01, ***p < 0.001. N ≥ 3 individuals for each group, unless specifically noted. See also Figure S2.

A

	Ochotona curzoniae (JAADBW010000000)	*Ochotona princeps* (OchPri 3.0)
GC%	44	44
Number of contigs	1779	10420
Total length (MB)	2012.1	1943.9
N50 size (MB)	33.9	24.3
Max size (MB)	84.8	73.8
BUSCO genome completeness	C: 93.0% [S: 92.4%, D: 0.6%], F: 1.9%, M: 5.1%, n: 9226	C: 90.2% [S: 89.5%, D: 0.7%], F: 2.3%, M: 7.5%, n: 9226

B

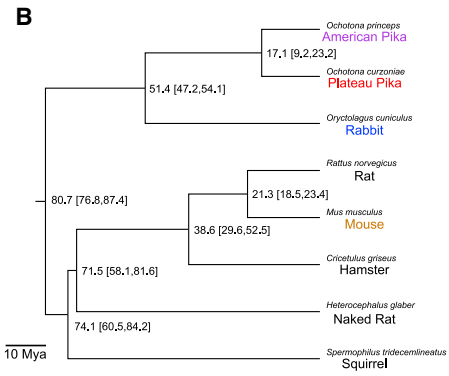

Figure 2. Genome-sequence comparisons of plateau and American pikas

(A) Summary statistics for the *de novo* genome assembly of a reference genome for plateau pika. Comparison of genomic sequences indicates that the quality of our newly generated data for the genome of plateau pika (*O. curzoniae*) is comparable to or even of higher quality than the previously reported genome for American pika (*O. princeps*).

(B) Gilres genome-similarity analysis and the estimated evolution time, based on the available genomic sequence data of *Lagomorpha* (pika and rabbit) and rodents (including rat and mouse).

De novo assembly and comparative analysis of Pl-Pika genome

We sequenced and assembled a *de novo* reference genome for Pl-Pika and compared it with the previously published Am-Pika genome. To assemble the genome of Pl-Pika, we used a hybrid-sequencing strategy by combining state-of-the-art technologies. We generated a total 447.8G base of useful sequencing data including 264.8G base PacBio long reads (average of 19.4 KB reads length), 44.2G base Nanopore long reads (average of 9.4 KB reads length), and 138.8G base Illumina short reads (150 nt pair-end reads, insert size 300 bp). Total genome coverage was up to 210× (genome size estimated to be ~2.0G base). The first version of our assembly (NCBI Bio project PRJNA601872, accession no. JAADBW010000000) resulted in a 2.0G base draft genome sequence, and the longest contig size was 84.8M base, and the N50 size was 33.9M base. Thus, the genome assembly showed excellent continuity and completeness (Figure 2A). To facilitate accurate annotation, we also conducted transcriptome sequencing from major organs (including the brain, heart, lung, liver, kidney, spleen, testis, and ovary), and we subsequently collaborated by sharing the sequencing with the NCBI group of the Eukaryotic Genome Annotation Pipeline and finished the annotation of the whole genome of Pl-Pika. We estimate that more than 98% genome sequences are covered by our assembly according to the mapping rate of independent RNA- and DNA-sequencing reads. Our initial genome annotation included 32,156 protein-coding genes, and approximately 99% of genes in the Am-Pika genome can be found in our annotation. Thus, we have obtained reliable genomic data for further molecular and genetic studies.

As expected, the genome of Pl-Pika was most similar to Am-Pika among the available Glires genomes, which consist of all those from known rodents and lagomorphs (Figure 2B). We observed that about 97.4% of our Pl-Pika genome sequences could be aligned to the published Am-Pika genome with an average of 90.5% identity. The genome divergence between Pl-Pika and Am-Pika species was more than between humans and chimpanzees but less than between mice and rats. Per evolutionary calculations based on our genome-sequencing information (Lindblad-Toh et al., 2011), we estimated that the divergence time of these two pika species was approximately 17.1 Mya (95% confidence [9.2, 23.2] Mya). These results are in line with the fossil-record-based prediction (>10 Mya). The divergence of the two pika species seems to have occurred earlier than the ancestor of Am-Pika crossing Beringia (2–3 Mya) and earlier than the QTP's dramatic uplift procession (~3 Mya).

The intracellular clockwork of Pl-Pika is disrupted

To further investigate the cellular clock machinery, we harvested primary fibroblast cells from ears of 2-month-old arrhythmic Pl-Pika animals. In addition, we used regular lab mice (C57BL/6J), rats, and rabbits to conduct parallel analyses. Each of these primary cells or those subsequently immortalized via SV40 large-T antigen infection (i.e., cell lines) was infected with lentiviral *Per2-dLuc* reporter that has been successfully used with human U2OS cells (Zhang et al., 2009). As shown, all mouse, rat, and rabbit primary cells revealed elegant cosine-wave oscillations of the *Per2* reporter expression. In contrast, the pika fibroblasts showed low amplitude and irregular rhythms, suggesting a disrupted or crippled clock in these pika cells (Figures 3A and S3A). This recording result was confirmed by a qPCR analysis of known clock genes such as *Bmal1*, *Per2*, *Cry1*, and *Nr1d1*, which are robustly rhythmic in rabbit fibroblasts but almost completely arrhythmic in pika fibroblasts, as evaluated using JTK_Cycle (Figure 3B).

Core-clock components of Pl-Pika possess normal functions individually

Compared with published mammalian genomes, we found no Pl-Pika-specific mutations among the core-clock genes, suggesting that its individual clock components may still be

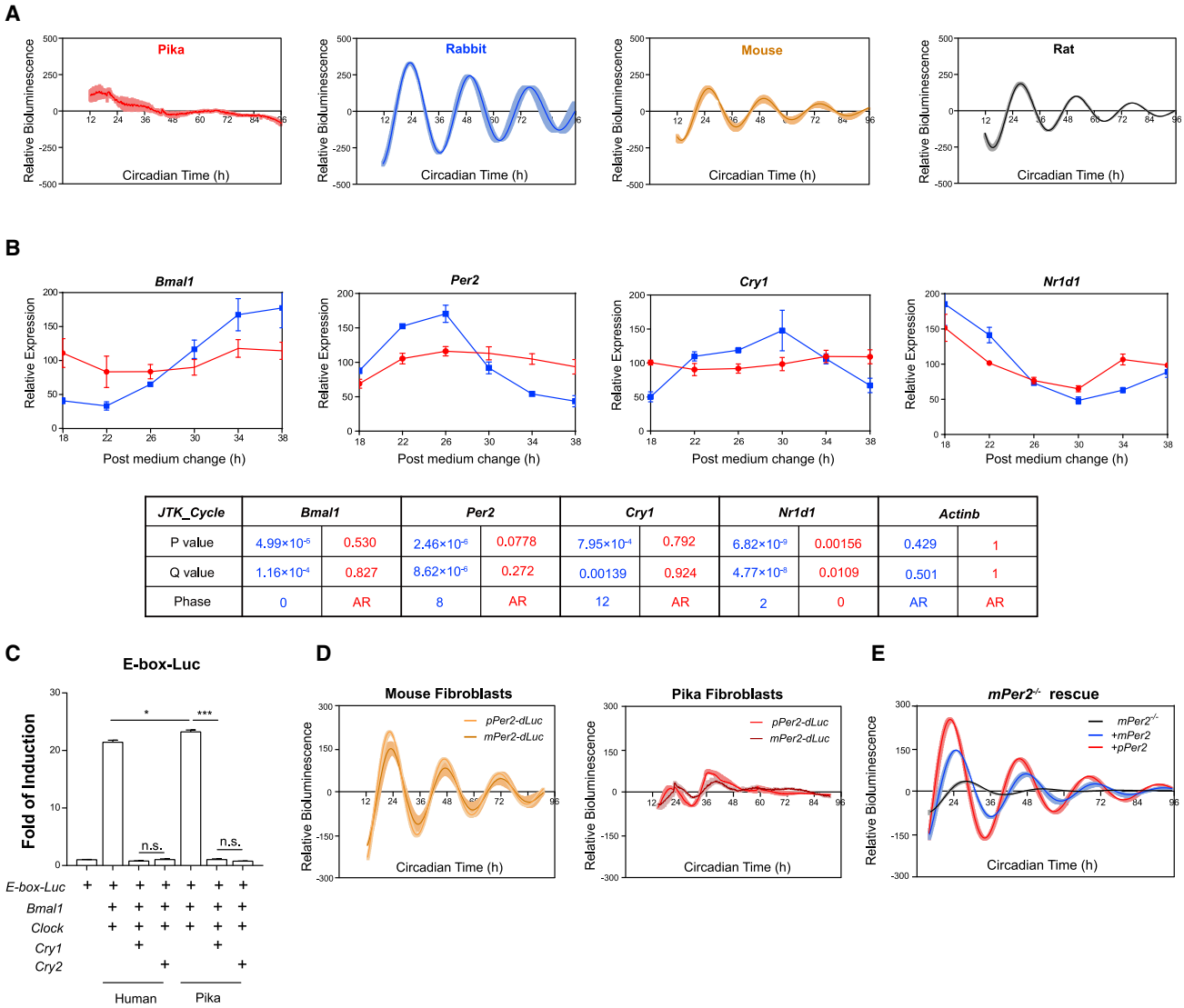

JTK_Cycle	Bmal1		Per2		Cry1		Nr1d1		Actinb	
P value	4.99×10^{-5}	0.530	2.46×10^{-6}	0.0778	7.95×10^{-4}	0.792	6.82×10^{-9}	0.00156	0.429	1
Q value	1.16×10^{-4}	0.827	8.62×10^{-6}	0.272	0.00139	0.924	4.77×10^{-8}	0.0109	0.501	1
Phase	0	AR	8	AR	12	AR	2	0	AR	AR

Figure 3. Pika fibroblasts express functional clock components, but their intracellular rhythmicity is disrupted

(A) A weak oscillation of *Per2-dLuc* in pika primary fibroblasts versus robust oscillations in rabbit, mouse, and rat primary fibroblast cells.

(B) Time course qPCR confirms that the expression of 4 known core-clock genes, *Bmal1*, *Per2*, *Cry1*, and *Nr1d1,* is robustly rhythmic in rabbits (blue) but not arrhythmic pika (red) primary fibroblast cells. Table: JTK_Cycle analysis was conducted to quantify and evaluate the rhythmicity of gene expression.

(C) Human and pika *Bmal1*, *Clock*, *Cry1*, and *Cry2* were compared using a luciferase transfection assay in human HEK 293T cells.

(D) A functional E-box in the promoter of the *Per2* genes of pika and mouse. The promoters were cloned into lentiviral vectors and subsequently infected into either mouse (left) or pika (right) fibroblast cell lines.

(E) A pika *Per2* minigene (with the native promoter driving its cDNA, shown in red) can rescue the rhythmicity of mouse *Per2*$^{-/-}$ fibroblasts (black). Positive control: a mouse *Per2* minigene also rescued the rhythmicity of mouse *Per2*$^{-/-}$ fibroblasts (blue).

Error bars represent SEM, and statistical significance was determined using two-sided Student's t tests when only two groups were analyzed. *$p < 0.05$, **$p < 0.01$, ***$p < 0.001$. $n \geq 3$ samples for each group, unless specifically noted.

See also Figure S3.

functional. We confirmed this assertion via a series of compensation studies. For instance, in a widely used luciferase transient-transfection assay, pika *Clock*, *Bmal1*, *Cry1*, and *Cry2* genes can induce the *E-box-Luc* signal as significantly as human and mouse orthologs (Figures 3C and S3B). In addition, the cloned pika *Per2* promoter fragment retains the capability to drive the luciferase oscillation in clock-intact mouse fibroblasts but not in clock-crippled pika cells (Figures 3D and S3C). Furthermore, we verified the function of pika *Per2* by re-introducing its minigene (the native promoter-driven cDNA) into *Per2*$^{-/-}$ mouse fibroblasts, which showed a nice rescue of the rhythm (Figures 3E and S3D). Together, these results demonstrate that the PI-Pika clock components are individually functional.

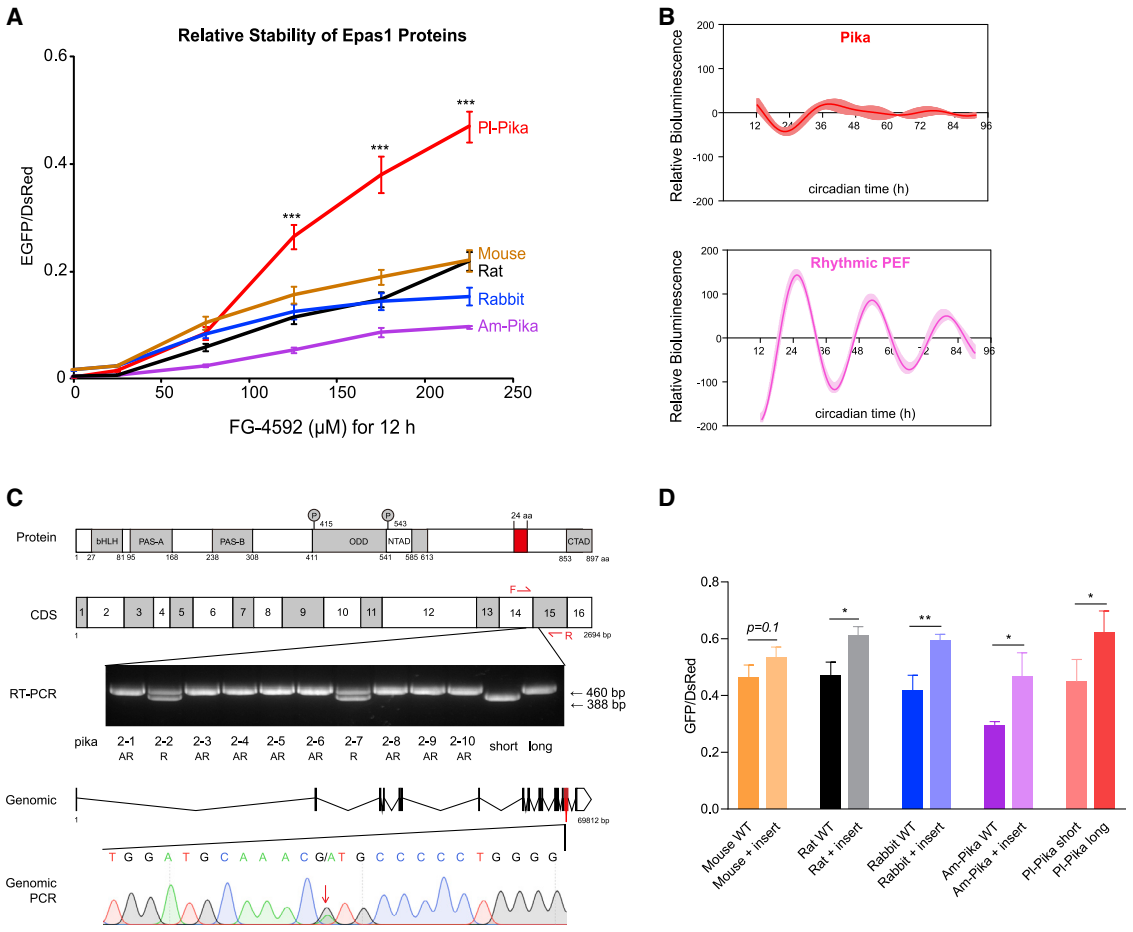

Figure 4. Multiple *Epas1* splice variants differentially regulate pika rhythmicity

(A) GPS analysis showing that the major isoform of plateau pika (Pl-Pika) Epas1 is more stable than Epas1 orthologs of other mammals.

(B) Above: cell line originated from arrhythmic Pl-Pika, in which the *Per2-dLuc* signal is arrhythmic. Below: cell line originated from pika embryo fibroblasts, in which the *Per2-dLuc* signal is rhythmic.

(C) A sequence alignment identified a unique insertion (in red) between Exon14 and Exon15 in the Pl-Pika Epas1 protein. The Pl-Pika-specific Epas1 insert identified is indicated with red. RT-PCR results showing that rhythmic pikas had both short and long isoform *Epas1* sequences, and genomic PCR showing they are heterozygous at the G/A site.

(D) GPS analysis showing that long-form Epas1 is more stable than the short isoform of rat, mouse, rabbit, American pika (Am-Pika), and Pl-Pika in HEK 293T cells.

Error bars represent SEM, and statistical significance was determined using two-sided Student's t test when only two groups were analyzed. *$p < 0.05$, **$p < 0.01$, ***$p < 0.001$. $n \geq 3$ samples for each group, unless specifically noted.

See also Figure S4.

Multiple *Epas1* splice variants differentially regulate pika rhythmicity

Our previous study showed that induction of hypoxia signals, which generally stabilize hypoxia-inducible factors (HIF proteins), can disrupt the clock in mouse suprachiasmatic nucleus (SCN) *ex vivo* cultures and in human U2OS cells (Wu et al., 2017). Therefore, we hypothesized whether any HIF variants in the Pl-Pika might contribute to its clock arrhythmicity. We carefully analyzed the amino-acid sequences of Hif-1α, Hif-2α/Epas1, and Hif-1β/Arnt from all published mammalian genomes, and the only Pl-Pika-specific polymorphic amino-acid residues among these were for the Epas1 protein (Table S3).

We next investigated whether the protein stability of Epas1 orthologs from mammals including rabbit, rat, mouse, and Am-Pika differ. Global protein stability (GPS) assays offer an unambiguous way to assess the stability of any given analyte protein (Yen et al., 2008) and have been successfully harnessed for circadian research (Liu and Zhang, 2016). We used this approach to evaluate Epas1 in normoxia (i.e., 21% oxygen) and hypoxia conditions with assays using HEK 293T cells. Compared with the stability of Epas1 proteins in other mammals, treatment of cells with the hypoxia-mimicking reagent FG-4592 (also with $NiCl_2$) caused a dramatic increase in the protein stability of the Pl-Pika, as evaluated by the EGFP/DsRED signal ratio (Figure 4A and S4A).

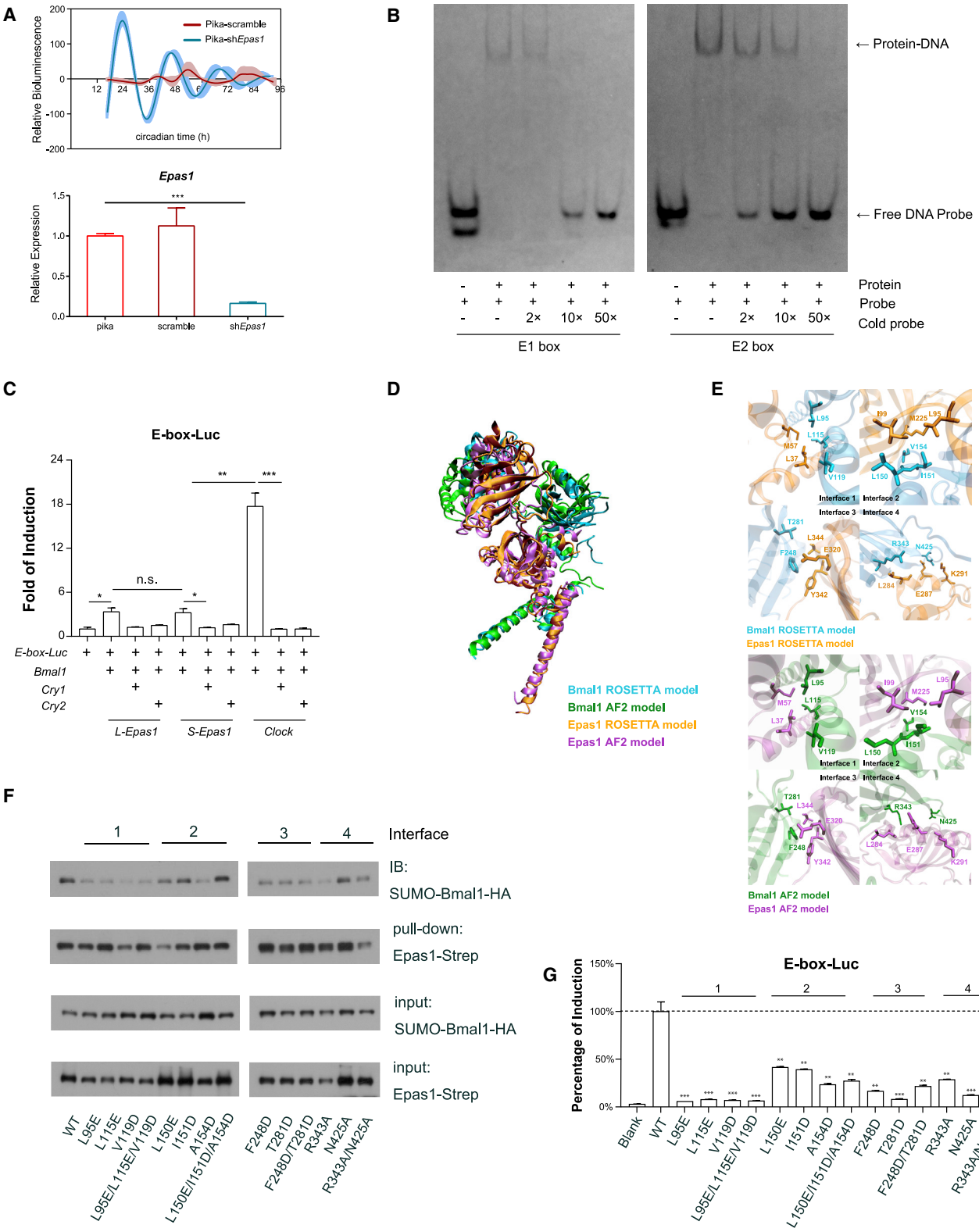

(legend on next page)

As reported in earlier sections, for PI-Pika individuals (Figure 1), we observed heterogeneity of rhythmicity and the possible participation of Epas1 in the regulation of circadian rhythm under hypoxic conditions. Therefore, we considered whether there are any differences in Epas1 sequence between arrhythmic and rhythmic pikas and other rhythmic mammals, which could build a linkage between Epas1 protein stability and animal rhythmicity.

Comparing the amino-acid sequence of *Epas1* in different species, it is evident that the PI-Pika *Epas1* has a unique insertion between Exon14 and Exon15 (Figure S4B). At the 5′ end of the insertion, there is a G > A mutation in arrhythmic PI-Pika, which may disrupt an RNA splicing site that could alter a splicing site (Figure S4C).

Fortunately, we obtained one cell line originating from pika embryo fibroblasts (PEFs), where both the *Per2-dLuc* signal (Figure 4B) and the gene expression of *Per2* (Figure S4D) are in good rhythmicity. Therefore, we cloned Epas1 from both genomic DNA and cDNA of the rhythmic and the arrhythmic pika cell lines and the behaviorally rhythmic or arrhythmic pikas. We observed that the rhythmic cell line and both the rhythmic pika individuals (all of the rhythmic ones were recorded in the second batch) harbored two forms of the *Epas1* cDNA sequence (a "short" 2,622 bp form, designated as *S-Epas1*, and a "long" 2,694 bp form, or *L-Epas1*). In sharp contrast, the arrhythmic cells and all arrhythmic individuals had only *L-Epas1* (Figures 4C and S4E). Genotypically, the rhythmic cells and animals were heterozygous at the 5′ end of the Intron14 G/A site. In contrast, the arrhythmic cells and animals were homozygous (i.e., a total of 18 As and 2 Gs in the 10 pika individuals examined; Figure 4C). These striking findings suggest a plausible mechanism that could explain the differential circadian rhythmicity among the PI-Pika population: genetic variation of nucleotide G2296A in the *Epas1* locus.

To verify the function of this specific 24-residue insert in Epas1 protein stability, we also used GPS assays to examine the stability of these two pika Epas1 isoforms: we observed significantly higher stability of PI-Pika L-Epas1 than S-Epas1 in the presence of hypoxia-mimicking reagent FG-4592. We further inserted this PI-Pika-specific 24 residue into the Epas1 orthologs in rabbit, rat, mouse, and Am-Pika (between Exon14 and Exon15); the results showed a significant increase in Epas1 protein stability, similar to that of PI-Pika L-Epas1 versus S-Epas1 (Figure 4D).

All this genomic, molecular genetics, and biochemical evidence support the hypothesis that the observed differential circadian rhythmicity of the PI-Pika population would ultimately be explained by heterozygosity at the Intron14 G/A site of the Epas1 locus that affects RNA splicing and protein stability in a manner that disrupts the circadian clockwork.

Biochemical and structural analyses reveal an Epas1-Bmal1 complex that can reside at E-box loci

To verify the effect of stabilized L-Epas1 variant in disturbing circadian rhythm, we used shRNA to knockdown *Epas1* in otherwise arrhythmic pika cells containing only the *L-Epas1*. The knockdown alone can credibly rescue the rhythmicity as assayed by *Per2-dLuc* bioluminescence recording (Figure 5A and S5A).

To characterize the complex of Epas1-Bmal1 with a *cis*-element DNA fragment derived from the Per2 promoter region (CACGTT/G) (Rey et al., 2011; Shimomura et al., 2013; Sobel et al., 2017), we applied electrophoretic mobility shift assay (EMSA) (Yoo et al., 2004). Purified pika Epas1 and Bmal1 were incubated with the classic E1/2-box motif DNA fragment. As shown in Figure 5B, Epas1 and Bmal1 heterodimerize and bind to E1/2-box.

Next, we mechanistically connected our insights about differential hypoxia-triggered Epas1 stability to the observed PI-Pika arrhythmicity. Our previous study showed that both stabilized human HIF1A (by pharmacological treatments) and BMAL1 can co-occupy the E-box element of the *Per2* promoter and impact the clock (Wu et al., 2017), and another study also indicated an interaction between HIF1A with clock proteins such as BMAL1 and CRY (Vaughan et al., 2020). Further, one other study showed that human EPAS1 interacts with the core-clock component BMAL1 and binds to the hypoxia-response element (HRE) (Saito et al., 2010). We therefore investigated if pika Epas1 binds with Bmal1 at E-box loci to initiate transcriptional activation.

We demonstrated that co-transfection of *Epas1* and *Bmal1* can modestly activate an E-box element-driven reporter to a much less degree than that of *Clock-Bmal1* co-transfection; additionally, the *E-box-Luc* signal induced by co-transfection

Figure 5. Biochemical and structural analyses of an EPAS1-BMAL1-E-box complex

(A) Knockdown *L-Epas1* in arrhythmic pika cells. The knockdown alone can rescue the rhythmicity.

(B) An EMSA assay revealing that the Epas1-Bmal1 protein complex can bind to the synthetic E1 (left) and E2 (right) elements of the *Per2* promoter. Cy5-labeled 21 bp DNA fragment was retarded in the gel by purified truncations of pika Epas1 and Bmal1 mixture (958 nM total protein, 1:1 molar ratio) while competitively released by the extra amount of free probes (100 nM as 1×).

(C) Transfection reporter assays examining Epas1-Bmal1-mediated activation from a synthetic DNA fragment (containing canonical E-box elements CACGTG). Note that the *trans*-activation activity of Epas1-Bmal1 is lower than Clock-Bmal1.

(D) Homology modeling of the pika Epas1-Bmal1 complex, based on a published crystal structure of mouse Epas1-Arnt (PDB: 4H10 and 4ZPK). ROSETTA homology model: Bmal1 in blue and Epas1 in orange; AlphaFold2 model: Bmal1 in green and Epas1 in purple.

(E) Four predicted interfaces for pika Epas1-Bmal1 from the homology modeling. ROSETTA homology model: Bmal1 in blue and Epas1 in orange; AlphaFold2 model: Bmal1 in green and Epas1 in purple.

(F) Pull-down assays with selected mutant variants of pika Bmal1 with the Epas1 truncation fragment to confirm the functional contributions of particular residues on Epas1-Bmal1 complex formation.

(G) These modeled interactions were verified by functional luciferase assay using mutants generated in the interface regions.

Error bars represent SEM, and statistical significance was determined using a two-sided Student's t test when only two groups were analyzed. *$p < 0.05$, **$p < 0.01$, ***$p < 0.001$. $n \geq 3$ samples for each group, unless specifically noted.

See also Figure S5.

of pika *L-Epas1* and *Bmal1* does not differ from co-transfection of pika *S-Epas1* and *Bmal1*, suggesting that *L-* or *S-Epas1* does not influence the transactivation activity of the Epas1-Bmal1 complex, both of which are significantly lower than the Clock-Bmal1 complex (Figure 5C).

We subsequently investigated how Epas1 interacts with Bmal1. Since the crystal structures of the Clock-Bmal1-E-box complex and the Epas1-Arnt complex have been individually reported, we performed homology modeling using these crystal structures (PDB: 4H10, 4ZPK) as the template (Figures 5D and S5B). We also predicted a few regions that participate in the interaction of these two proteins conserved with the reported Epas1-Arnt structure (Wu et al., 2015) and that are known to impact the association of HIF1a (a close homolog of Epas1) with Bmal1 (Vaughan et al., 2020) (Figure 5E). Further, after the publication of AlphaFold2, we immediately utilized this tool to generate a predicted model independently of our homology modeling. We used the amino-acid sequences of Epas1 and Bmal1, which we connected (computationally) with a poly-proline linker (40 residues) (Ko and Lee, 2021). The AlphaFold2 model matched our previous homology modeling very well (Table S4) in general and in the four predicted interfaces (Figures 5D and 5E).

These modeled interactions were subsequently successfully verified by a series of biochemical pull-down assays and functional luciferase assays using Bmal1 variants bearing mutations at the predicted interface regions (14 mutants in total; Figures 5F and 5G). Using the homology modeling results, we also conducted molecular-dynamic modeling to refine the structure (Figure S5B), and subsequently, we compared the binding energy of PAS domains of Epas1-Bmal1 or Clock-Bmal1 complex via umbrella sampling (Lemkul and Bevan, 2010). The results showed that the binding of Epas1-Bmal1 is slightly higher than Clock-Bmal1 (Figure S5C), indicating that Epas1 might probably compete with Clock and dimerize with Bmal1.

These findings together support a plausible explanation for how the increased stability of the L-Epas1 could interface with the circadian clockwork to yield the observed arrhythmicity phenotypes in the PI-Pika population. Specifically, the increased cellular population of Epas1 resulting from its increased stability would increase the extent of Epas1-Bmal1 complex formation, and given our finding that the Epas1-Bmal1 complex has reduced lower *trans*-activation ability compared with Clock-Bmal1, the molecular regulatory consequence of increased Epas1 stability would be decreased overall transcription from E-box-containing loci, which would disrupt the expression of E-box-driven circadian genes, thus disrupting the pika rhythms.

Expression of PI-Pika *L-Epas1* into mice recaptures the arrhythmic phenotype

To investigate the physiological function of PI-Pika *L-Epas1 in vivo*, we generated a knockin mouse line expressing its coding sequence in the *Epas1* locus using CRISPR-Cas9 technology (Figure S6A). In parallel, we also generated knockin mice expressing proteasome-sensitive rat *Epas1* to ensure that the stabilized form of Epas1, but not the knockin procedure itself, produced the cellular or animal phenotype.

First, we conducted a chromatin immunoprecipitation (ChIP)-qPCR assay to verify that the Epas1 co-localized with Bmal1 at the promoter of *Per2*, as well as *Epas1* itself, indicating the participation of Epas1 in the circadian circuit in the knockin mouse fibroblasts (Figure S6B).

Next, we evaluated whether the L-Epas1 knockin impacted the central clock located in the SCN. These mice were bred with a Per2::LUC reporter line, and subsequently, the SCN explants were derived for *ex vivo* culture. We showed that the pika *L-Epas1* knockin SCN was more sensitive to hypoxic agents for the Per2::LUC oscillation (Figures 6A–6C). The *Per2* reporter dampened quickly upon treatment, and the amplitude dramatically reduced.

We asked whether the pika *L-Epas1* knockin mice may exhibit disrupted body-temperature rhythms, as observed in the PI-Pika animals. However, after examining more than 50 offspring from the heterozygous breed, we could not obtain homozygous pika *L-Epas1*-expressing mice, suggesting its apparent embryonic lethality. We dissected pregnant mice to examine the embryogenesis of these genetically modified mice and found that the homozygous pika *L-Epas1* knockin is lethal at embryonic day 11.5 (E11.5)–E15.5 (Figure S6C). The control rat *Epas1* knockin mice, harboring a proteasome-sensitive isoform of Epas1, were normal and born under expected Mendelian ratios. The heterozygous pika *L-Epas1* knockin mice are viable but do not have impaired body-temperature rhythms in the hypoxia condition (Figure S6D).

To explore the physiological functions of pika L-Epas1 in the central clock, we microinjected an associated virus (adeno-associated virus [AAV]) for the expression of pika *L-Epas1* into the mouse SCN (Figure S7A), and SCN microinjection of AAV-rat *Epas1* was used as a control. Mice core-body-temperature recordings revealed that those microinjected with AAV-pika *L-Epas1* exhibited significantly less robust core-body-temperature rhythms without a significant change in the average level at 10% O_2 conditions than the control group (Figures 7A–7D and S7B–S7E). We conclude that a stabilizing form of Epas1 in the SCN can jeopardize daily physiological rhythms such as body temperature, particularly in low-oxygen conditions.

Knockin of pika L-Epas1 in mice protects the heart from hypoxia-induced damage

To examine whether pika *L-Epas1* is sufficient to mimic the highland adaptation of the PI-Pika to the hypoxic condition, we housed the unmanipulated wild-type C57, pika *L-Epas1,* or rat *Epas1* knockin mice in chambers with hypoxia (10% O_2) or normaxia (21% O_2) conditions for 1 month and measured the chronic impacts of the low-oxygen environment. Reportedly, this treatment would result in body-weight loss, hypoxia-induced hypertension, right ventricle hypertrophy (RVH) in regular mice, and elevated hemoglobin (Huerta-Sánchez et al., 2014; Peng et al., 2017). We observed that wild-type (WT) and rat *Epas1* knockin mice, but not pika *L-Epas1* knockin mice, exhibited more severe loss of body weight and increase of hemoglobin level (hyperhemoglogineamia) after 1 month of housing in the 10% oxygen chamber compared with their littermate controls in the normoxic chamber (Figures 7E and 7F). In addition, WT and rat *Epas1* knockin mice also developed RVH, which is not

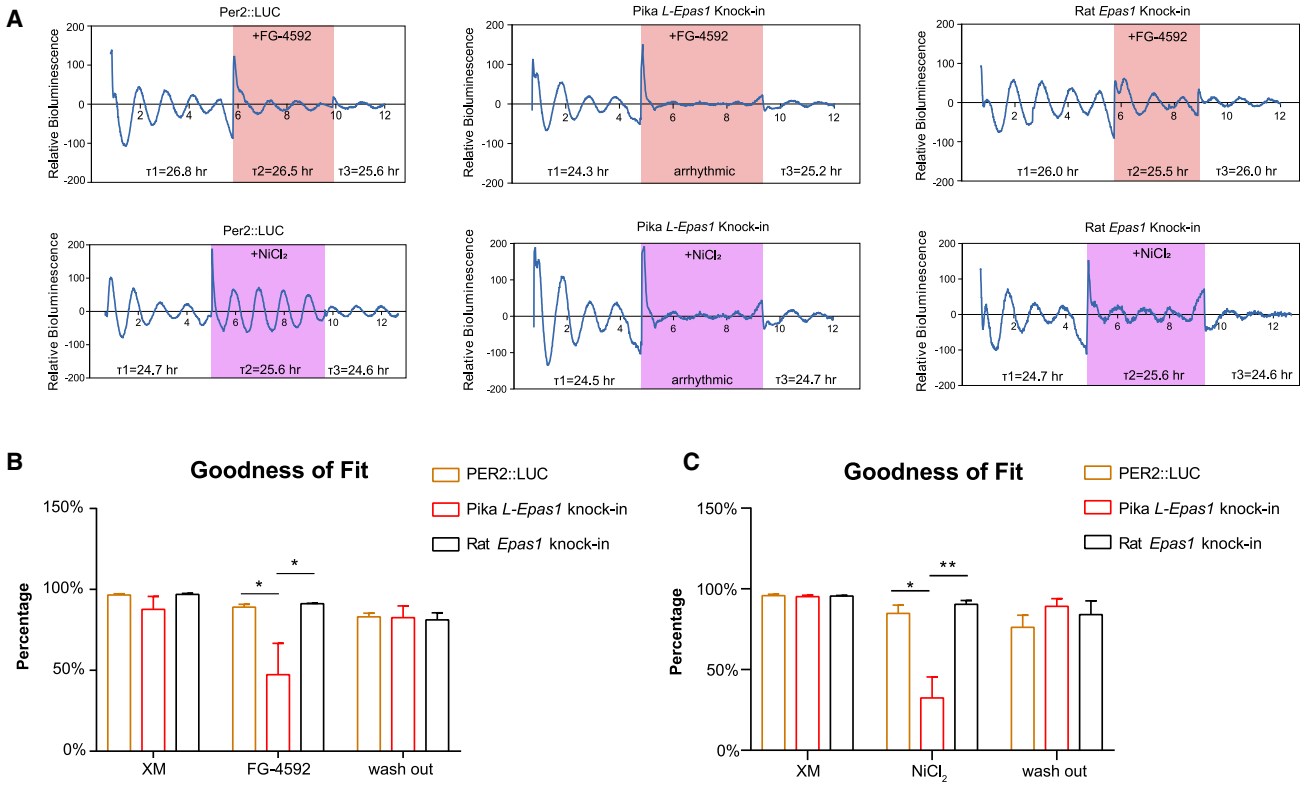

Figure 6. *Ex vivo* analyses of *Epas1* knockin mice

(A) *Ex vivo* cultures of SCN prepared from the knockin mice, indicating that pika Epas1 interferes with the mouse SCN clock in the presence of the hypoxia-mimic agents FG-4592 or $NiCl_2$.

(B and C) Rhythmicity analyses of robustness for the clocks of FG-4592- or $NiCl_2$-treated SCN *ex vivo*.

Error bars represent SEM, and statistical significance was determined using two-sided Student's t tests when only two groups were analyzed. *$p < 0.05$, **$p < 0.01$, ***$p < 0.001$. $n \geq 3$ samples for each group, unless specifically noted.

See also Figure S6.

evident in pika *L-Epas1* knockin mice (Figures 7G–7I). Together, these results suggest that pika *L-Epas1* knockin mice are better adapted to the hypoxic environment.

DISCUSSION

This study attempts to address how the PI-Pika population is largely arrhythmic. We started by observing arrhythmic behavior and physiology in pika individuals, then proceeded to genetic and molecular dissection and identified a point mutation in the PI-Pika *Epas1* locus, which altered splicing and thus increased protein stability. We subsequently clarified the participation of Epas1 in circadian regulation and highlighted the stabilized Epas1 protein as the key point for disrupting the rhythmicity in the majority of PI-Pikas. In the end, we came back to the individual level by demonstrating that knockin mice with the pika *L-Epas1* developed a disrupted circadian clock and adapted to a low-oxygen environment.

We identified a key G/A mutation in Intron14 of the PI-Pika *Epas1* gene, resulting in a 24-residue insert stabilizing the Epas1 protein. This insert is unique to the PI-Pika and has never been reported. We hypothesized that this is the key point that makes the majority of PI-Pikas arrhythmic to better adapt to harsh living conditions. This mutation is not the only one responsible for highland adaption. For example, Tibetans have multiple intronic SNP sites in *Epas1*, presumably affecting its expression (Buroker et al., 2012), and Tibetan horses have a possibly more stable variant of the Epas1 protein (Liu et al., 2019). Here, we established the relationship between Epas1 stability and circadian rhythmicity.

We believe that the stabilized Epas1 and disrupted circadian clock are natural selections in the PI-Pika (for PAML analysis, see Table S3). Besides the heart-protection advantages and relatively low hyper-hemoglobineamia in hypoxic environments, the disrupted circadian rhythm (caused by stabilized Epas1) may also contribute to PI-Pika survival on the QTP. Circadian clocks are thought to provide the ability to anticipate daily temperature and food-availability changes, thereby maximizing energy expenditure to fit the environmental LD cycles (Dunlap, 1999). However, the ambient-temperature change could be very dynamic and irregular in the QTP and could hardly be "anticipated." For example, dramatic temperature reduction in the daytime (could be ~20°C in minutes) could be detrimental for anticipators with the circadian clock. If the pika makes an incorrect "prediction" of the temperature via its robust internal clock, it could be at risk of hypothermia and may not survive under

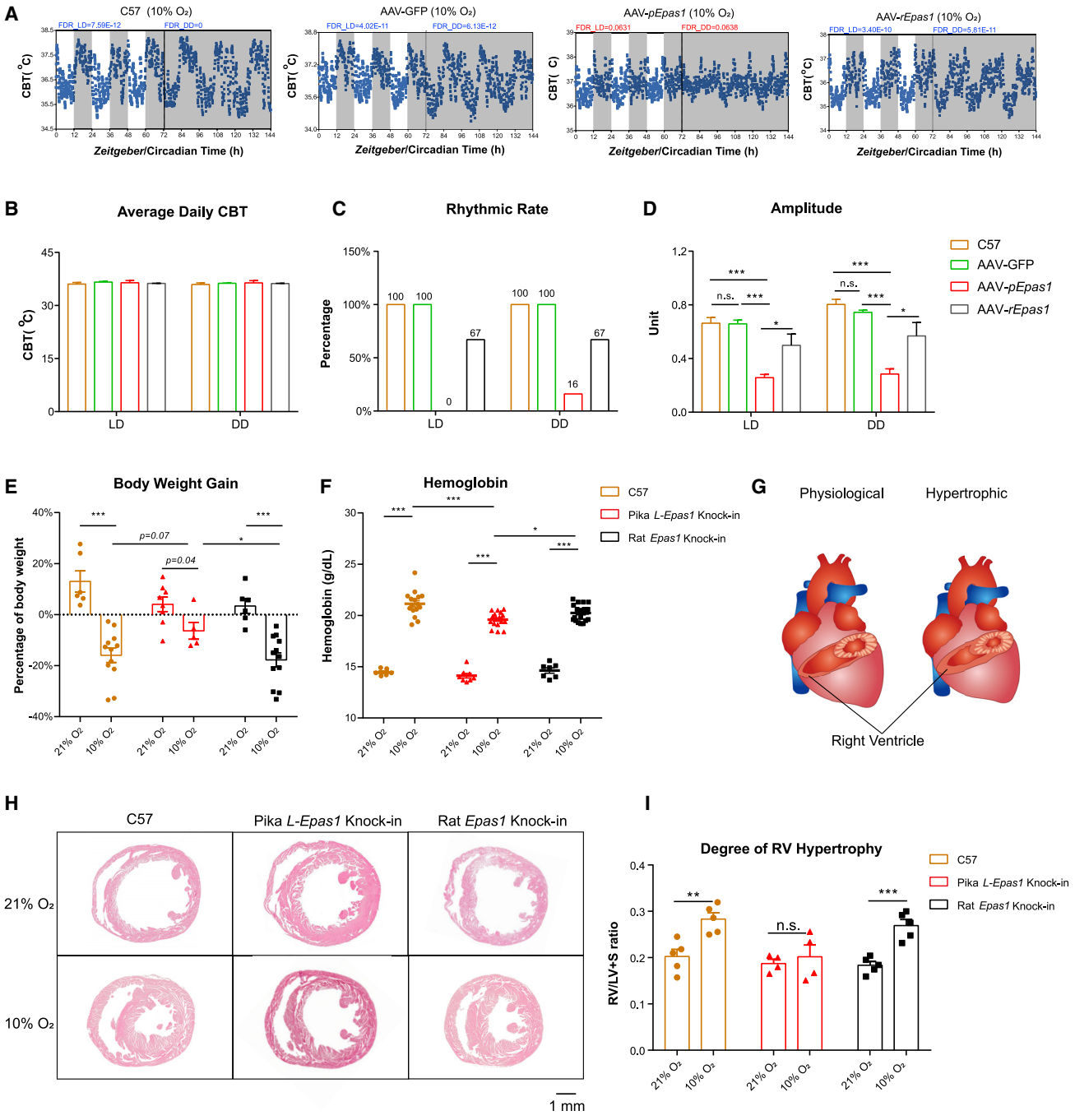

Figure 7. Adaptations of pika *L-Epas1* expressed mice to 10% O_2 environment

(A) Representative curves of longitudinal CBT recording from mice bearing the SCN of AAV-*Epas1* injection in a sealed chamber with 10% O_2 conditions, mimicking the QTP hypoxic environment.

(B–D) Analyses of average core body temperatures and assessment of the robustness of their daily rhythmic variability.

(E) Pika, rat *Epas1* knockin, and unmanipulated WT mice were maintained in the normaxic (21% O_2) or hypoxic (10% O_2) chambers for 1 month, and their body weights were measured; unlike the other two groups of control animals, the pika *L-Epas1* knockin mice did not lose weight in the hypoxic condition.

(F) Hemoglobin was measured in mice under normoxic (21% O_2) or hypoxic (10% O_2) conditions.

(G) A cartoon illustrating typical murine right ventricle hypertrophy sites, adapted from Türck et al. (2018).

(H) Representative images of H&E staining for pathological analysis.

(I) Right ventricle hypertrophy assays confirmed the reduced damage of the pika *L-Epas1* knockin mice compared with control mice.

Error bars represent SEM, and statistical significance was determined using two-sided Student's t tests when only two groups were analyzed. *$p < 0.05$, **$p < 0.01$, ***$p < 0.001$. $N \geq 3$ individuals for each group, unless specifically noted.

See also Figure S7.

such capricious conditions. Thus, hypothermia, coupled with drastic irregular temperature changes, exterts negative selection pressure against the circadian clock in the pika and probably other QTP species.

High-altitude adaptation is critical for mammals living in areas 2,500 m or more above sea level. In human genome-wide association studies, people in the Andean plateau of South America and the Ethiopia plateau of Africa use a mechanism involving *HBB* (encoding the hemoglobin) to adapt to high altitude (Alkorta-Aranburu et al., 2012; Beall, 2007). Conversely, the Tibetan population harbors two specific SNPs in the *EPAS1* and *EGLN1* (a negative regulator of HIF proteins) gene loci, suggesting that the HIF-mediated signals play a central role in response to this extreme living condition (Lorenzo et al., 2014; Simonson et al., 2010). Similarly, polymorphisms in the *Epas1* gene can also be found in Tibetan dogs (Wang et al., 2014). In the present study, we demonstrate that PI-Pikas, the most populous mammal widely distributed in most of the QTP area, harbors a gene variant encoding a stabilized form of Epas1. It would be interesting to uncover how Tibetan mammals, probably convergently, evolved to utilize the Epas1-mediated pathway to adapt to this very plateau (the QTP, but not other highlands) environment. Our discovery of the loss of circadian rhythms in the pika may provide a potential explanation for circadian involvement.

Finally, given the now recognized biological significance of cross-talk between hypoxia signaling and circadian regulation, we expect that the molecular insights from this study support deeper/better understanding of physiological and pathological events in humans, including erythropoietin (EPO) production, heart function, anaerobic glucose utilization during exercise, the brain's responses to sleep apnea, and even cancer development (Adamovich et al., 2017; Dimova et al., 2019; Peek et al., 2017; Vaughan et al., 2020; Walton et al., 2018; Wu et al., 2017).

Limitations of the study

In this study, we observed the heterogeneity of PI-Pika in circadian rhythm and identified a mutation in the Epas1 gene that altered splicing of Epas1, affecting protein stability, and thus resulted in heterogeneity of rhythmicity. Our study focused primarilyy on experiments with caged animals, which may not fully reflect the wild environment. Some evidence (albeit indirect) bears consideration here: recall from above that previous ecological studies of the PI-Pika have reported inconsistent findings as to whether this animal is diurnal, crepuscular, etc. Nevertheless, there is consensus among QTP ecological researchers that the PI-Pika is a keystone species and that it is the most populous mammal in the landscape. The PI-Pika is the primary food source for nearly all meat-eating predators of the QTP, including consensus diurnal animals (e.g., upland buzzard, alpine weasel), nocturnal animals (Eurasian eagle, little owl), and crepuscular animals (Tibetan fox, brown bear). These food-web ideas also suggest that the PI-Pika population does not display strongly rhythmic behaviors in the wild (Smith et al., 2019).

Although we used several biochemical and cellular approaches to study the stability and degradation of the Epas1 protein, further studies of the differential degradation of the L- and S-Epas1 proteins are warranted. Finally, it should be noted that we used computational modeling combined with biochemical assays to investigate the Epas1-Bmal1-E-box interaction; additional biochemical experiments (e.g., microscale thermophoresis [MST] and surface plasmon resonance [SPR]) could be applied conducted to compare the binding affinity of the Epas1-Bmal1 complex with the Clock-Bmal1 complex, which could advance understanding of how Epas1 disrupts the circadian system.

STAR★METHODS

Detailed methods are provided in the online version of this paper and include the following:

- KEY RESOURCES TABLE
- RESOURCE AVAILABILITY
  - Lead contact
  - Materials availability
  - Data and code availability
- EXPERIMENTAL MODEL AND SUBJECT DETAILS
  - Animals
  - Generation of mouse models
  - Cell lines and cell culture
- METHOD DETAILS
  - Rhythmicity analysis
  - Lentiviral constructs and stable cell line generations
  - LumiCycle recording of infected fibroblasts and data analysis
  - Time course qPCR
  - Transient transfection and luciferase assay
  - Global protein stability profiling (GPS)
  - Electrophoresis mobility shift assays (EMSA) and fluorescence anisotropy assays
  - Plasmid construction and protein purification
  - Western blot
  - Homology modeling and molecular dynamics
  - Streptavidin affinity pull-down
  - ChIP-qPCR
  - LumiCycle recording of SCN
  - Recombinant adeno-associated virus generation
  - Stereotactic surgery and core body temperature recording
  - Weight loss ratio
  - Hemoglobin detection
  - HE staining
  - Assessment of right ventricular hypertrophy
- QUANTIFICATION AND STATISTICAL ANALYSIS

SUPPLEMENTAL INFORMATION

Supplemental information can be found online at https://doi.org/10.1016/j.celrep.2022.110816.

ACKNOWLEDGMENTS

We thank the NCBI group of "Eukaryotic Genome Annotation Pipeline" for helping with pika genome annotation. The authors would like to make special thanks to Drs. G. Wu at Cincinnati Children's Hospital, T.L. Leise at Amherst

College, and D.K. Welsh at UCSD for circadian-robustness analyses in cells and animals. We are also grateful to Drs. S.J. Elledge at Harvard for providing the GPS vectors, S. Hattar at NIMH for stimulating discussion, D. Ju in E.E.Z.'s lab for technical support, and A.L. Zhang of Canyon Crest Academy and J.H. Snyder of BPF Consulting for writing assistance. The research was supported by funds from the Ministry of Science and Technology of the People's Republic of China (2021ZD0203400 to E.E.Z.); the National Natural Science Foundation of China (31971090 to E.E.Z., 32100938 to N.L., 31860293 to W.W., and 81972360 to S.L.); the Beijing Municipal Government and Tsinghua University (to E.E.Z.); the "Second Tibetan Plateau Scientific Expedition and Research Program" (no. 2019 QZKK0501 to Y.Z.) and the "Project of Western Light for Interdisciplinary Team" of CAS (to Y.Z.); and Hubei Province Department of Education (Q20182501 to N.L.).

AUTHOR CONTRIBUTIONS

N.L. and E.E.Z. conceived the study; N.L., H.T., Z.Y., and E.E.Z. designed the experiments; N.L., H.T., Z.Y., and Y.C. performed the molecular/cellular experiments; W.L. captured pika animals in the wild field and conducted behavioral and core body temperature (CBT) experiments with H. Zhang in Y.Z.'s laboratory; H. Zhao purified proteins and conducted biochemical assays with help from Z.G. and W.W. under guidance from S.Z.; Z.Y. performed homology and AlphaFold modeling assays; H.T. performed the mouse work with M.L., Z.X., C.C., Y.G., and Y.W.; F.W. generated the knock-in mice; T.C. analyzed the sequencing data along with H.-w.H., J.W., and K.L.; D.S. summarized the evolution of the Genus pika; N.L., H.T., and Z.Y. analyzed all other experimental results; H.H. and S.L. provided financial support to H.T.; W.W. offered scientific inputs; E.E.Z. oversaw the project; and Z.Y. and E.E.Z. wrote the manuscript, which all authors commented on.

DECLARATION OF INTERESTS

The authors declare no competing interests.

Received: November 15, 2020
Revised: February 7, 2022
Accepted: April 20, 2022
Published: May 17, 2022

REFERENCES

Adamovich, Y., Ladeuix, B., Golik, M., Koeners, M.P., and Asher, G. (2017). Rhythmic oxygen levels reset circadian clocks through HIF1α. Cell Metab. *25*, 93–101. https://doi.org/10.1016/j.cmet.2016.09.014.

Alkorta-Aranburu, G., Beall, C.M., Witonsky, D.B., Gebremedhin, A., Pritchard, J.K., and Di Rienzo, A. (2012). The genetic architecture of adaptations to high altitude in Ethiopia. PLoS Genet. *8*, e1003110. https://doi.org/10.1371/journal.pgen.1003110.

Balsalobre, A., Damiola, F., and Schibler, U. (1998). A serum shock induces circadian gene expression in mammalian tissue culture cells. Cell *93*, 929–937. https://doi.org/10.1016/s0092-8674(00)81199-x.

Beall, C.M. (2007). Two routes to functional adaptation: Tibetan and Andean high-altitude natives. Proc. Natl. Acad. Sci. U S A *104*, 8655–8660. https://doi.org/10.1073/pnas.0701985104.

Berendsen, et al. (1995). GROMACS: A message-passing parallel molecular dynamics implementation. Comp. Phys. Comm. *91*, 43–56. https://doi.org/10.1016/0010-4655(95)00042-E.

Buroker, N.E., Ning, X.H., Zhou, Z.N., Li, K., Cen, W.J., Wu, X.F., Zhu, W.Z., Scott, C.R., and Chen, S.H. (2012). EPAS1 and EGLN1 associations with high altitude sickness in Han and Tibetan Chinese at the Qinghai-Tibetan Plateau. Blood. Cells Mol. Dis. *49*, 67–73. https://doi.org/10.1016/j.bcmd.2012.04.004.

Dawson, M.R. (1969). Osteology of prolagus sardus, a Quaternary Ochotonid (mammalia, lagomorpha). Palaeovertebrata *2*, 157–190. https://doi.org/10.18563/pv.2.4.157-190.

Dimova, E.Y., Jakupovic, M., Kubaichuk, K., Mennerich, D., Chi, T.F., Tamanini, F., Oklejewicz, M., Hänig, J., Byts, N., Mäkelä, K.A., et al. (2019). The circadian clock protein CRY1 Is a negative regulator of HIF-1α. iScience *13*, 284–304. https://doi.org/10.1016/j.isci.2019.02.027.

Dunlap, J.C. (1999). Molecular bases for circadian clocks. Cell *96*, 271–290. https://doi.org/10.1016/s0092-8674(00)80566-8.

Huerta-Sánchez, E., Jin, X., Asan, B.Z., Peter, B.M., Vinckenbosch, N., Liang, Y., Yi, X., He, M., Somel, M., Ni, P., et al. (2014). Altitude adaptation in Tibetans caused by introgression of Denisovan-like DNA. Nature *512*, 194–197. https://doi.org/10.1038/nature13408.

Hughes, M.E., Hogenesch, J.B., and Kornacker, K. (2010). JTK_CYCLE: an efficient nonparametric algorithm for detecting rhythmic components in genome-scale data sets. J. Biol. Rhythms *25*, 372–380. https://doi.org/10.1177/0748730410379711.

Jumper, J., Evans, R., Pritzel, A., Green, T., Figurnov, M., Ronneberger, O., Tunyasuvunakool, K., Bates, R., Žídek, A., Potapenko, A., et al. (2021). Highly accurate protein structure prediction with AlphaFold. Nature *596*, 583–589. https://doi.org/10.1038/s41586-021-03819-2.

Ko, J., and Lee, J. (2021). Can AlphaFold2 predict protein-peptide complex structures accurately?. Preprint at bioRxiv. https://doi.org/10.1101/2021.07.27.453972.

Lanier, H.C., and Olson, L.E. (2009). Inferring divergence times within pikas (Ochotona spp.) using mtDNA and relaxed molecular dating techniques. Mol. Phylogenet. Evol. *53*, 1–12. https://doi.org/10.1016/j.ympev.2009.05.035.

Leise, T.L. (2017). Analysis of nonstationary time series for biological rhythms research. J. Biol. Rhythms *32*, 187–194. https://doi.org/10.1177/0748730417709105.

Lemkul, J.A., and Bevan, D.R. (2010). Assessing the stability of alzheimer's amyloid protofibrils using molecular dynamics. J. Phys. Chem. B *114*, 1652–1660. https://doi.org/10.1021/jp9110794.

Lin, Z., Chen, L., Chen, X., Zhong, Y., Yang, Y., Xia, W., Liu, C., Zhu, W., Wang, H., Yan, B., et al. (2019). Biological adaptations in the Arctic cervid, the reindeer (Rangifer tarandus). Science *364*, aav6312. https://doi.org/10.1126/science.aav6312.

Lindblad-Toh, K., Garber, M., Zuk, O., Lin, M.F., Parker, B.J., Washietl, S., Kheradpour, P., Ernst, J., Jordan, G., Mauceli, E., et al. (2011). A high-resolution map of human evolutionary constraint using 29 mammals. Nature *478*, 476–482. https://doi.org/10.1038/nature10530.

Liu, A.C., Welsh, D.K., Ko, C.H., Tran, H.G., Zhang, E.E., Priest, A.A., Buhr, E.D., Singer, O., Meeker, K., Verma, I.M., et al. (2007). Intercellular coupling confers robustness against mutations in the SCN circadian clock network. Cellule *129*, 605–616. https://doi.org/10.1016/j.cell.2007.02.047.

Liu, N., and Zhang, E.E. (2016). Phosphorylation regulating the ratio of intracellular CRY1 protein determines the circadian period. Front. Neurol. *7*, 159. https://doi.org/10.3389/fneur.2016.00159.

Liu, X., Zhang, Y., Li, Y., Pan, J., Wang, D., Chen, W., Zheng, Z., He, X., Zhao, Q., Pu, Y., et al. (2019). EPAS1 gain-of-function mutation contributes to high-altitude adaptation in Tibetan horses. Mol. Biol. Evol. *36*, 2591–2603. https://doi.org/10.1093/molbev/msz158.

López Martínez, N. (2001). Paleobiogeographical history of Prolagus, an European ochotonid (Lagomorpha). Lynx (Praha), 215–231.

Lorenzo, F.R., Huff, C., Myllymäki, M., Olenchock, B., Swierczek, S., Tashi, T., Gordeuk, V., Wuren, T., Ri-Li, G., McClain, D.A., et al. (2014). A genetic mechanism for Tibetan high-altitude adaptation. Nat. Genet. *46*, 951–956. https://doi.org/10.1038/ng.3067.

Luo, Z., Matsumoto, T., Ohwatari, N., Shimazu, M., and Kosaka, M. (1997). Insulative adaptation to cold and absence of circadian body temperature rhythm in afghan pikas : ochotona rufescens rufescens. Trop. Med. *38*, 107–116.

Parati, G., Agostoni, P., Basnyat, B., Bilo, G., Brugger, H., Coca, A., Festi, L., Giardini, G., Lironcurti, A., Luks, A.M., et al. (2018). Clinical recommendations for high altitude exposure of individuals with pre-existing cardiovascular

conditions. Eur. Heart J. *39*, 1546–1554. https://doi.org/10.1093/eurheartj/ehx720.

Peek, C.B., Levine, D.C., Cedernaes, J., Taguchi, A., Kobayashi, Y., Tsai, S.J., Bonar, N.A., McNulty, M.R., Ramsey, K.M., and Bass, J. (2017). Circadian clock interaction with HIF1α mediates oxygenic metabolism and anaerobic glycolysis in skeletal muscle. Cell Metab. *25*, 86–92. https://doi.org/10.1016/j.cmet.2016.09.010.

Peng, Y., Cui, C., He, Y., Ouzhuluobu, Z.H., Yang, D., Zhang, Q., Bianbazhuoma, Y.L., He, Y., Xiang, K., Zhang, X., et al. (2017). Down-regulation of EPAS1 transcription and genetic adaptation of tibetans to high-altitude hypoxia. Mol. Biol. Evol. *34*, msw280–msw830. https://doi.org/10.1093/molbev/msw280.

Plummer, C.C., Carlson, D.H., and Hammersley, L. (2016). Physical Geology, Fifteenth editon (McGraw-Hill Education).

Rey, G., Cesbron, F., Rougemont, J., Reinke, H., Brunner, M., and Naef, F. (2011). Genome-wide and phase-specific DNA-binding rhythms of BMAL1 control circadian output functions in mouse liver. PLoS Biol. *9*, e1000595. https://doi.org/10.1371/journal.pbio.1000595.

Rose, K.D., DeLeon, V.B., Missiaen, P., Rana, R.S., Sahni, A., Singh, L., and Smith, T. (2008). Early eocene lagomorph (mammalia) from western India and the early diversification of Lagomorpha. Proc. Biol. Sci. *275*, 1203–1208. https://doi.org/10.1098/rspb.2007.1661.

Royden, L.H., Burchfiel, B.C., and van der Hilst, R.D. (2008). The geological evolution of the Tibetan plateau. Science *321*, 1054–1058. https://doi.org/10.1126/science.1155371.

Saito, T., Fukai, A., Mabuchi, A., Ikeda, T., Yano, F., Ohba, S., Nishida, N., Akune, T., Yoshimura, N., Nakagawa, T., et al. (2010). Transcriptional regulation of endochondral ossification by HIF-2α during skeletal growth and osteoarthritis development. Nat. Med. *16*, 678–686. https://doi.org/10.1038/nm.2146.

Shimomura, K., Kumar, V., Koike, N., Kim, T.K., Chong, J., Buhr, E.D., Whiteley, A.R., Low, S.S., Omura, C., Fenner, D., et al. (2013). Usf1, a suppressor of the circadian Clock mutant, reveals the nature of the DNA-binding of the CLOCK:BMAL1 complex in mice. Elife *2*, e00426. https://doi.org/10.7554/elife.00426.

Simonson, T.S., Yang, Y., Huff, C.D., Yun, H., Qin, G., Witherspoon, D.J., Bai, Z., Lorenzo, F.R., Xing, J., Jorde, L.B., et al. (2010). Genetic evidence for high-altitude adaptation in tibet. Science *329*, 72–75. https://doi.org/10.1126/science.1189406.

Smith, A.T., Badingqiuying, W.M.C., and Hogan, B.W. (2019). Functional-trait ecology of the plateau pika Ochotona curzoniae in the Qinghai-Tibetan Plateau ecosystem. Integr. Zool *14*, 87–103. https://doi.org/10.1111/1749-4877.12300.

Smith, A.T., Gemma, F., Xie, Y., Hoffmann, R.S., Lunde, D., and MacKinnon, J. (2010). A Guide to the Mammals of China (Princeton University Press).

Sobel, J.A., Krier, I., Andersin, T., Raghav, S., Canella, D., Gilardi, F., Kalantzi, A.S., Rey, G., Weger, B., Gachon, F., et al.; CycliX consortium (2017). Transcriptional regulatory logic of the diurnal cycle in the mouse liver. PLoS Biol. *15*, e2001069. https://doi.org/10.1371/journal.pbio.2001069.

Tiscornia, G., Singer, O., and Verma, I.M. (2006). Production and purification of lentiviral vectors. Nat. Protoc. *1*, 241–245. https://doi.org/10.1038/nprot.2006.37.

Türck, Patrick, et al. (2018). Trapidil improves hemodynamic, echocardiographic and redox state parameters of right ventricle in monocrotaline-induced pulmonary arterial hypertension model. Biomed. Pharmacother. *103*, 182–190. https://doi.org/10.1016/j.biopha.2018.04.001.

van Oort, B.E.H., Tyler, N.J.C., Gerkema, M.P., Folkow, L., Blix, A.S., and Stokkan, K.-A. (2005). Circadian organization in reindeer. Nature *438*, 1095–1096. https://doi.org/10.1038/4381095a.

Vaughan, M.E., Wallace, M., Handzlik, M.K., Chan, A.B., Metallo, C.M., and Lamia, K.A. (2020). Cryptochromes suppress HIF1α in muscles. iScience *23*, 101338. https://doi.org/10.1016/j.isci.2020.101338.

Walton, Z.E., Patel, C.H., Brooks, R.C., Yu, Y., Ibrahim-Hashim, A., Riddle, M., Porcu, A., Jiang, T., Ecker, B.L., Tameire, F., et al. (2018). Acid suspends the circadian clock in hypoxia through inhibition of mTOR. Cell *174*, 72–87.e32. https://doi.org/10.1016/j.cell.2018.05.009.

Wang, G.D., Fan, R.X., Zhai, W., Liu, F., Wang, L., Zhong, L., Wu, H., Yang, H.C., Wu, S.F., Zhu, C.L., et al. (2014). Genetic convergence in the adaptation of dogs and humans to the high-altitude environment of the Tibetan plateau. Genome Biol. Evol. *6*, 2122–2128. https://doi.org/10.1093/gbe/evu162.

Wang, J.M., Zhang, Y.M., and Wang, D.H. (2006). Seasonal thermogenesis and body mass regulation in plateau pikas (Ochotona curzoniae). Oecologia *149*, 373–382. https://doi.org/10.1007/s00442-006-0469-1.

Wang, Z., Wu, Y., Li, L., and Su, X.D. (2013). Intermolecular recognition revealed by the complex structure of human CLOCK-BMAL1 basic helix-loop-helix domains with E-box DNA. Cell. Res. *23*, 213–224. https://doi.org/10.1038/cr.2012.170.

Wu, D., Potluri, N., Lu, J., Kim, Y., and Rastinejad, F. (2015). Structural integration in hypoxia-inducible factors. Nature *524*, 303–308. https://doi.org/10.1038/nature14883.

Wu, G., Anafi, R.C., Hughes, M.E., Kornacker, K., and Hogenesch, J.B. (2016). MetaCycle: an integrated R package to evaluate periodicity in large scale data. Bioinformatics *32*, 3351–3353. https://doi.org/10.1093/bioinformatics/btw405.

Wu, Y., Tang, D., Liu, N., Xiong, W., Huang, H., Li, Y., Ma, Z., Zhao, H., Chen, P., Qi, X., and Zhang, E.E. (2017). Reciprocal regulation between the circadian clock and hypoxia signaling at the genome level in mammals. Cell Metab. *25*, 73–85. https://doi.org/10.1016/j.cmet.2016.09.009.

Yen, H.-C.S., Xu, Q., Chou, D.M., Zhao, Z., and Elledge, S.J. (2008). Global protein stability profiling in mammalian cells. Science *322*, 918–923. https://doi.org/10.1126/science.1160489.

Yoo, S.-H., Yamazaki, S., Lowrey, P.L., Shimomura, K., Ko, C.H., Buhr, E.D., Siepka, S.M., Hong, H.-K., Oh, W.J., Yoo, O.J., et al. (2004). PERIOD2::LUCIFERASE real-time reporting of circadian dynamics reveals persistent circadian oscillations in mouse peripheral tissues. Proc. Natl. Acad. Sci. U S A *101*, 5339–5346. https://doi.org/10.1073/pnas.0308709101.

Yu, N., Zheng, C., Zhang, Y.-P., and Li, W.-H. (2000). Molecular systematics of pikas (Genus Ochotona) inferred from mitochondrial DNA sequences. Mol. Phylogenet. Evol. *16*, 85–95. https://doi.org/10.1006/mpev.2000.0776.

Zhang, E.E., and Kay, S.A. (2010). Clocks not winding down: unravelling circadian networks. Nat. Rev. Mol. Cell Biol. *11*, 764–776. https://doi.org/10.1038/nrm2995.

Zhang, E.E., Liu, A.C., Hirota, T., Miraglia, L.J., Welch, G., Pongsawakul, P.Y., Liu, X., Atwood, A., Huss, J.W., III, Janes, J., et al. (2009). A Genome-wide RNAi screen for modifiers of the circadian clock in human cells. Cell *139*, 199–210. https://doi.org/10.1016/j.cell.2009.08.031.

Zheng, B., Larkin, D.W., Albrecht, U., Sun, Z.S., Sage, M., Eichele, G., Lee, C.C., and Bradley, A. (1999). The mPer2 gene encodes a functional component of the mammalian circadian clock. Nature *400*, 169–173. https://doi.org/10.1038/22118.

Zielinski, T., Moore, A.M., Troup, E., Halliday, K.J., and Millar, A.J. (2014). Strengths and limitations of period estimation methods for circadian data. PLoS One *9*, e96462. https://doi.org/10.1371/journal.pone.0096462.

STAR★METHODS

KEY RESOURCES TABLE

REAGENT or RESOURCE	SOURCE	IDENTIFIER
Antibodies		
Anti-rabbit HRP-linked secondary	Cell Signaling	Cat# 7074; RRID: AB_2099233
Anti-mouse HRP-linked secondary	Cell Signaling	Cat# 7076; RRID: AB_330924
Anti-Bmal1 antibody - ChIP Grade	Abcam	Cat# ab3350; RRID: AB_303729
Mouse anti-HA	Thermo Fisher Scientific	Cat# 26183; RRID: AB_10978021
Streptactin Beads 4FF	Smart LifeSciences	Cat# 053005
Anti-strep-tag II antibody	Abcam	Cat# ab76949; RRID: AB_1524455
Superdex Columns	GE Healthcare	Cat# 28-9909-44
Bacterial and virus strains		
Virus: pAAV-hSyn-EGFP-WPRE-pA	Shanghai Taitool Bioscience Co.Ltd	Cat# S0237-9
Virus: pAAV- EF1a-Pika *L-Epas1*-V5	This paper	N/A
Virus: pAAV-EF1a-Rat *Epas1*-V5	This paper	N/A
BL21(DE3) Chemically Competent Cell	TransGen	Cat# CD601-02
Trans1-T1 Phage Resistant Chemically Competent Cell	TransGen	Cat# CD501-02
Chemicals, peptides, and recombinant proteins		
HIF Inhibitors	Selleck Chemicals	Cat# FG-4592
$NiCl_2$	JSENB	Cat# JS0319
IPTG	AMRESCO	Cat# 0487
PMSF	AMRESCO	Cat# 0754
Hematoxylin solution	Sigma-Aldrich	Cat# 03,971
Eosin Y solution	Sigma-Aldrich	Cat# 318906
Protease inhibitors, Complete Mini, EDTA-free	Roche	Cat# 11836170001
B27	Thermo Fisher	Cat# 17504044
D-luciferin, potassium salt	Goldbio	Cat# 115144-35-9
Critical commercial assays		
Bright- Glo™ Luciferase Assay System	Promega	Cat# E2620
ChIP-IT High Sensitivity Kit	Active Motif	Cat# 53040
2x rapid Taq master mix	Vazyme	Cat# P222-AA
KAPA HiFi Hotstart	KAPA Bio Systems	Cat# KB2500
Lipofectamine 2000	Thermo Fisher	Cat# 12566014
Lipofectamine 3000	Thermo Fisher	Cat# L3000015
PrimeScript™ RT Master Mix	Takara	Cat# RR036A
SsoAdvanced™ Universal SYBR® Green Supermix	BioRad	Cat# 1725275
M5 SuperFast Seamless Cloning Mix	Mei5Bio	Cat# MF017
Invitrogen clonase Gateway LR Clonase II Enzyme Mix	Thermo Scientific	Cat# 11791020
Deposited data		
genome assembly	NCBI Genome database	JAADBW000000000
Experimental models: Cell lines		
HEK-293T cells	ATCC	RRID: CVCL_0063
Pl-Pika fibroblasts	This paper	N/A
Pl-Pika embryo fibroblasts	This paper	N/A

(*Continued on next page*)

Continued

REAGENT or RESOURCE	SOURCE	IDENTIFIER
mouse fibroblasts	This paper	N/A
Rat fibroblasts	This paper	N/A
Rabbit fibroblasts	This paper	N/A
Per2$^{-/-}$ mouse fibroblasts	This paper	N/A
sf9 insect cells	ATCC	RRID: CRL-1711
Rat *Epas1* knock-in mouse fibroblasts	This paper	N/A
Pika *L-Epas1* knock-in mouse fibroblasts	This paper	N/A
Experimental models: Organisms/strains		
Mouse: C57BL/6J	The Jackson Laboratory	JAX Stock#: 000664
Mouse: mPer2^{Luc}: B6.129S6-*Per2*^{tm1Jt}/J	Yoo et al. (2004)	JAX Stock#: 006852
Mouse: *Per2*$^{-/-}$	Zheng et al. (1999)	N/A
Mouse: Pika *L-Epas1* knock-in	This paper	N/A
Mouse: Rat *Epas1* knock-in	This paper	N/A
Oligonucleotides		
Primers for RT-PCR/qPCR detection, see Table S2	This paper	N/A
shRNA for VHL or Epas1 knock down, see Table S2	This paper	N/A
Primers for *L/S-Epas1* detection, see Table S2	This paper	N/A
Primers for the heterozygous G/A site cloning and sequencing, see Table S2	This paper	N/A
Cy5 labeled E1/2-box forward strand (5′-GTTTGGTCACGTG/TTTCCACTA-3′)	This paper	N/A
Recombinant DNA		
Plasmid: pGL3-SV40-Ebox-*dLuc*	This paper	N/A
Plasmid: pGL3-P (mouse *Per2*)-*dLuc*	This paper	N/A
Plasmid: pcDNA3.1-CMV-3F6H-mouse *Clock*	This paper	N/A
Plasmid: pcDNA3.1-CMV-3F6H-mouse *Bmal1*	This paper	N/A
Plasmid: pcDNA3.1-CMV-3F6H-mouse *Cry1*	This paper	N/A
Plasmid: pcDNA3.1-CMV-3F6H-mouse *Cry2*	This paper	N/A
Plasmid: pcDNA3.1-CMV-3F6H-mouse *Epas1*	This paper	N/A
Plasmid: pcDNA3.1-CMV-3F6H-pika *Clock*	This paper	N/A
Plasmid: pcDNA3.1-CMV-3F6H-pika *Bmal1*	This paper	N/A
Plasmid: pcDNA3.1-CMV-3F6H-pika *Cry1*	This paper	N/A
Plasmid: pcDNA3.1-CMV-3F6H-pika *Cry2*	This paper	N/A
Plasmid: pcDNA3.1-CMV-3F6H-pika *L-Epas1*	This paper	N/A
Plasmid: pcDNA3.1-CMV-3F6H-pika S-*Epas1*	This paper	N/A
Plasmid: pcDNA3.1-CMV-3F6H-human *Clock*	This paper	N/A
Plasmid: pcDNA3.1-CMV-3F6H-human *Bmal1*	This paper	N/A
Plasmid: pcDNA3.1-CMV-3F6H-human *Cry1*	This paper	N/A

(*Continued on next page*)

Continued

REAGENT or RESOURCE	SOURCE	IDENTIFIER
Plasmid: pcDNA3.1-CMV-3F6H-human *Cry2*	This paper	N/A
Plasmid: pcDNA3.1-CMV-3F6H-human *Epas1*	This paper	N/A
Plasmid: pcDNA3.1-CMV-3F6H-EGFP	This paper	N/A
Plasmid: pLKO-U6-sh*Epas1*	This paper	N/A
Plasmid: pCDH-P(Pika *Per2*)-Pika *Per2*-EF1a-GFP	This paper	N/A
Plasmid: pCDH-P(mouse *Per2*)-mouse *Per2*-EF1a-GFP	This paper	N/A
Plasmid: pCDH-P(mouse *Per2*)-*dLuc*-EF1a-RFP	This paper	N/A
Plasmid: pCDH-P(Pika *Per2*)-*dLuc*-EF1a-RFP	This paper	N/A
Plasmid: pREV	Tiscornia et al. (2006)	N/A
Plasmid: pVSVG	Tiscornia et al. (2006)	N/A
Plasmid: pMDL	Tiscornia et al. (2006)	N/A
Plasmid: pCMV-DsRed-IRES-EGFP	Yen et al. (2008)	N/A
Plasmid: pET28a-6×His-SUMO-pika *Bmal1*	This paper	N/A
Plasmid: pET21a-strep-pika *Epas1*	This paper	N/A
Plasmid: pAAV-EF1a-Pika *L-Epas1*-V5	This paper	N/A
Plasmid: pAAV-EF1a-Rat *Epas1*-V5	This paper	N/A
Software and algorithms		
LumiCycle analysis	Actimetrics	N/A
BioDare2	Zielinski et al. (2014)	https://biodare2.ed.ac.uk
MetaCycle	Wu et al. (2016)	https://github.com/gangwug/MetaCycle
Unicorn5.11	cytiva	https://www.cytivalifesciences.com/en/us/shop/unicorn-5-11-p-03388
JTK Cycle	Hughes et al. (2010)	https://openwetware.org/mediawiki/index.php?title%20=%20=HughesLab:JTK_Cycle&oldid%20=%20=971822
Clock lab software	Actimetrics	N/A
PRISM	GraphPad	https://www.graphpad.com/scientific-software/prism/
Microsoft Excel	Microsoft	N/A
AlphaFold v2	Jumper et al. (2021)	https://github.com/deepmind/alphafold
ROSETTA	Rosetta Commons	https://www.rosettacommons.org/software
GROMACS	Berendsen et al. (1995)	http://www.gromacs.org/
Other		
SDS-PAGE loading buffer (6X)	Beyotime	Cat# P0015F
Thermo Scientific Pierce IP Lysis Buffer	Thermo Fisher Scientific	Cat# 87788
TRIzol™ Reagent	Thermo Fisher	Cat# 15596018
DAPI	Sigma-Aldrich	Cat# D9542
DMEM	Gibco	Cat# 11965092
RPMI 1640 Medium	Gibco	Cat# 22400089
Opti-MEM® I Reduced-Serum Medium (1X), liquid	Invitrogen	Cat# 51985034
Archimed X6 qPCR machine	RocGene Tecnology Co.	N/A

(*Continued on next page*)

Continued

REAGENT or RESOURCE	SOURCE	IDENTIFIER
AKTA Frac-950 Fraction Collector	Amersham Biosciences	N/A
MissionHb	ACON	N/A
E-mitter	Starr Life Sciences	G2

RESOURCE AVAILABILITY

Lead contact

Further information and requests for resources and reagents should be directed to and will be fulfilled by the lead contact, Eric Erquan Zhang (zhangerquan@nibs.ac.cn).

Materials availability

All unique reagents generated in this study are available from the lead contact upon request.

Data and code availability

The accession number for the sequencing data reported in this paper is NCBI Bioproject PRJNA601872, accession JAADBW000000000. This paper does not report original code. Any additional information required to reanalyze the data reported in this work paper is available from the lead contact upon request.

EXPERIMENTAL MODEL AND SUBJECT DETAILS

Animals

All animal works were performed following the guidelines of Institutional Animal Care and Use Committees (IACUC) at National Institute of Biological Sciences (NIBS) and Northwest Institute of Plateau Biology (NWIPB), Chinese Academy of Sciences. Specifically, adults of Plateau Pika were captured in the wild-field of Mt. Datong (Latitude: 37°30′31″ N; Longitude: 100°28′19″ E; Elevation: 3,580 m) of Qinghai province, China. We have harvested pikas from the wild-field twice in two different seasons, and conducted in-house experiments with total 20 pika individuals (#1-1∼1-10 in July, and #2-1∼2-10 in January. 6–14 months old, 16 male pikas, 4 female pikas). Temperature in the field varies widely (from summer daily 5–25°C to winter −25∼-5°C), and the average light duration ranges from 14.5h (summer) to 9.5h (winter) per day. Pika animals were subsequently housed in a facility room of NWIPB (Latitude: 36°37′38" N; Longitude: 101°44′58″ E; Elevation: 2,280m) with natural light-dark cycles (LD, 12h:12h; light intensity 108 lux) for two weeks before measuring their behavior and physiology under LD or completely covered by dark curtains (DD) conditions. They were single-caged and fed with regular Rabbit Complete Fodder (Keao-Xieli Feed Co.), and this in-house maintenance condition has been successfully used for more than 15 years (Wang et al., 2006). Wistar rats (∼4 months old, 15 male rats), as control animals, were bred and housed at NWIPB for more than 20 generations. The successful rate of surgeries for telemetric-transmitter implanting was 80–90% for each species. Mouse behavioral studies were carried out in the NIBS vivarium as described.

Generation of mouse models

PER2:LUC mice were purchased from the Jackson Laboratory (Yoo et al., 2004), and *Per2* knock-out mice were a generous gift from Dr. Ying Xu in Soochow University (Zheng et al., 1999). For generation of pika/rat *Epas1* knock-in mice, CRIPSR-Cas9 was used to insert the coding sequence of *Epas1* of pika or rat after the start codon of the first exon of *Epas1* of Per2:LUC mice with C57 background so that only the inserted *Epas1*, but not the original mouse *Epas1*, is expressed. For the gRNA used in generation of knock-in mice, see Table S2.

Cell lines and cell culture

HEK 293T cells (ATCC), and all mouse, rat, and rabbit (key resources table) were cultured at 37°C with a 5% CO_2 atmosphere in Dulbecco's Modified Eagle's Medium (DMEM, Thermo Fisher) supplemented with 10% fetal bovine serum (Gibco) and 1% Penicillin Streptomycin mixture (PS, Thermo Fisher). Plateau pika fibroblast and Plateau pika embryo fibroblast cells were cultured at 37°C with a 5% CO_2 atmosphere in RPMI 1640 Medium (Thermo Fisher) supplemented with 10% fetal bovine serum (Gibco) and 1% Penicillin Streptomycin mixture (PS, Thermo Fisher).

METHOD DETAILS

Rhythmicity analysis

The core body temperature of pika, rat, C57, pika *L-Epas1* knock-in mouse and rat *Epas1* knock-in mouse were analyzed with BioDare2 (Zielinski et al., 2014) and MetaCycle (Wu et al., 2016) software packages. (A) BioDare2: In analyzing period and phase,

FFT NLLS was used, and the expected periods were set to 20-28h. In rhythmicity analysis, BD2 eJTK was used. (B) MetaCycle: Data were analyzed mainly following the instructions, and the LombScargle method was used.

Lentiviral constructs and stable cell line generations

Lentivirus used was produced according to previous study (Tiscornia et al., 2006). Briefly, HEK293T cells were transfected with Lipofectamine 3000 (Thermo Fisher) strictly following the manufacturer's instructions. 4 μg of plasmid DNA was transfected into each well of 6 well-plate or 3.5 cm dish (2.23 μg of packaging plasmids mixture, with the mass ratio pMDL:pVSVG:pREV = 270:176:95, and for cell lines for LumiCycle recording, 1.77 μg pCDH-*Per2-dLuc*-EF1a-RFP with *Per2* promoter of mouse or pika; for cell lines for *Per2* overexpression, pCDH-P(*Per2*)-*Per2*-EF1a-EGFP with both the promoter and *Per2* CDS from mouse or pika; for *Epas1* knock-down, 1.77 μg of pLKO-U6-shRNA/scramble, for shRNA sequence, see Table S2). The supernatant containing lentivirus was collected 48h after transfection, cleared of debris by filtering through a 0.45 μm filter, and then transferred to the plate containing target cell lines. Infected cells were sorted with flow cytometry, and the knock-down efficiency was detected via qPCR (for primers, see Table S2).

LumiCycle recording of infected fibroblasts and data analysis

Cells were planted in 3.5 cm dishes. When grown confluent, DMEM was replaced with the explant media (DMEM supplement with 0.1 mM D-luciferin, pen/strep and 5% B27 supplement). Cells were then placed into LumiCycle (ACTIMETRICS) to record for 5-9 days. Data were subtracted and analyzed by LumiCycle Analysis.

Time course qPCR

Cells reached confluence before synchronized using serum shock (Balsalobre et al., 1998). Briefly, the medium was exchanged by serum-rich medium (49% DMEM, 1% PS, 50% horse serum [GIBCO]), and exchanged by serum-free medium (99% DMEM, 1% PS) 2 h later. After 18 h, cells were harvested and were harvested every 4 h thereafter, for a total of 6 times. After RNA extraction using TRIzol (Thermo Fisher), RT-qPCR were used to assess the expression of core circadian genes. For primers used in qPCR, see Table S2. Rhythmicity was analyzed by JTK_Cycle (Hughes et al., 2010).

Transient transfection and luciferase assay

HEK293T cells (ATCC) were transfected with Lipofectamine 3000 (Thermo Fisher) strictly following the manufacturer's instructions. Briefly, 200 ng of plasmid DNA was transfected into each well of 96 well-plates (For luciferase assays in Figures 3 and S3, 10 ng pGL3.1-SV40-Ebox-*dLuc*, 40 ng pcDNA3.1-3F6H-pika/human/mouse *Clock/Epas1*, 70 ng pcDNA3.1-3F6H- pika/human/mouse *Bmal1*, 10 ng pcDNA3.1-3F6H-pika/human/mouse *Cry1/Cry2*, and appropriate pcDNA3.1-3F6H-EGFP to 200 ng. For luciferase assays in Figure 5, 10 ng pGL3.1-SV40-Ebox-*dLuc*, 80 ng pcDNA3.1-3F6H-pika *Clock/L-Epas1/S-Epas1*, 20 ng pcDNA3.1-3F6H-pika *Bmal1*, 90 ng pcDNA3.1-3F6H-pika *Cry1/Cry2*, and appropriate pcDNA3.1-3F6H-EGFP to 200 ng.). Cells were incubated for 48h post-transfection before the luciferase assay. Luciferase assay was performed with Bright-Glo Luciferase Assay System (Promega) strictly following the manufacturer's instructions.

Global protein stability profiling (GPS)

All control vectors were a generous gift from Dr. Stephen J. Elledge (Yen et al., 2008). The coding sequence of *Epas1* of Pl-Pika, Am-Pika, rat, rabbit and mouse were cloned onto PGAW-GPS vectors before the plasmids were transfected into HEK293T cells using Lipofectamine 3000 (Thermo Fisher). FG-4592 or $NiCl_2$ were added when cells were 60% confluent. A total of 1×10^4 DsRED-positive cells were obtained through fluorescence-activated cell sorting and the half-life of Epas1 of different species were represented by the ratio between EGFP and DsRED-expressing cells.

Electrophoresis mobility shift assays (EMSA) and fluorescence anisotropy assays

For EMSA, the fluorescent double strand DNA containing pika *Per2* E1-box or E2-box was prepared by annealing Cy5 labeled forward strand (5′-GTTTGGTCACGTG/TTTCCACTA-3′) with the unlabeled reverse strand (5′-CTAGTGGAAC/AACGTGACCAAA) in the buffer consisting of 10 mM Tris pH 8.0, 60 mM NaCl, 1 mM EDTA. The annealed double strand DNA probe and cold probe competitors (as control) (100 nM as 1×) were incubated with purified complex proteins (958 nM total protein, 1:1 molar ratio) in the reaction buffer (50 mM Tris pH 7.5, 45 mM NaCl) for 15 min at room temperature. The samples were then loaded on an 5% non-denaturing polyacrylamide gels and run at constant voltage of 10 V/cm in 0.5× TBE buffer at 4°C. The gels were directly scanned on a ChemiDoc MP (BIO-RAD) imaging system.

Plasmid construction and protein purification

For the protein expression in *E.coli*, 6×His-SUMO tagged truncated pika Bmal1 (residues 68-453) and StrepII tagged truncated Epas1 (residues 3-361) were cloned into pET28a and pET21a vectors, respectively, and co-transformed into BL21 competent cells. Following the IPTG (100 μM) induced overnight expression at 16°C, cell pellets were lysed by sonication in a lysis buffer A containing 20 mM HEPES pH 7.5, 300 mM NaCl, 5 mM β-Mercaptoethanol, 10%(v/v) glycerol, 2 mM PMSF, and supernatant samples after centrifugation were applied onto a Streptactin beads (Smart LifeSciences) equilibrated with the lysis buffer A and the bound protein

was eluted with buffer G (20 mM HEPES pH 7.5, 150 mM NaCl, 2.5 mM Desthiobiotin). Purification was monitored by SDS-PAGE and Coomassie brilliant blue staining.

Bmal1-6×His-StrepII and Epas1-eGFP-6×His-protein c bacmids for residues 68-453 of pika Bmal1 and residues 3-361 of pika Epas1, respectively, were transfected into sf9 insect cells to produce recombinant P1 baculovirus. The cells were infected with P2 virus at a density of 1.5 x 10^6 cells/mL in ESF 921 insect cell culture medium (Expression Systems) and grown at 27°C for 60 h before collection. The cell pellets were resuspended in lysis buffer (20 mM HEPES, 300 mM NaCl, 10 mM $CaCl_2$, 5%(v/v) glycerol, 2 mM PMSF, 2 mM DTT; pH 7.5) and sonicated on ice for 20 min. Monoclonal mouse antibody Anti-Protein C was covalently coupled to NHS-activated Sepharose 4 FF beads (Cytiva) before use. The clarified cell lysate was applied onto the coupled beads) equilibrated with the lysis buffer and washed with a wash buffer (20 mM HEPES, 300 mM NaCl, 2 mM $CaCl_2$, 5%(v/v) glycerol, 2 mM DTT; pH 7.5). The bound protein was eluted with a buffer (20 mM HEPES, 300 mM NaCl, 100 μg/mL Protein C Peptide, 5%(v/v) glycerol, 5 mM EDTA, 2 mM DTT; pH 7.5). The Bmal1:Epas1 complex was further purified using a HiTrap Heparin HP column (Cytiva).

Western blot

Protein sample was separated by SDS–PAGE and transferred to a polyvinylidene difluoride membrane at 400 mA for 100-120 min at 4°C. Membranes were blocked at room temperature in TBST containing 5% nonfat-milk for 1h and then incubated overnight at 4°C with anti-strep (Sigma, 1:3500) or anti-HA (Thermo Fisher Scientific, 1:8000). After washed with TBST, the membranes were incubated with secondary antibodies conjugated to horseradish peroxidase against rabbit or mouse IgG (Cell Signaling,1:2500). Finally, the blot signal was detected with Immobilon ECL substrate (Millipore) and captured using X-Ray films. The protein level of each sample was normalized with input.

Homology modeling and molecular dynamics

The homology modeling was performed with ROSETTA software mainly according to instructions. Briefly, the crystal structure of mouse Arnt (PDB id: 4ZPK) (Wu et al., 2015) was used as the template of mouse Bmal1 homology modeling. The sequences of mouse Arnt and mouse Bmal1 were aligned using an online tool clustalo (http://www.ebi.ac.uk/Tools/msa/clustalo/). The fragment library of Bmal1 was generated at robetta.bakerlab.org. A total of 500 models were generated, and a best model was determined according to its score and goodness of fit to Epas1 interface. Breaks in crystal structures were closed and refined with ROSETTA loop modeling protocol and remodel protocol. For the amino acid sequence of bHLH-PAS domains of Epas1 or Bmal1 of mouse, human and pika was highly conserved except for a few mutations, the mouse Epas1-Bmal1 complex was then mutated to pika using ROSETTA loop modeling and remodel protocol. The complex was aligned with the crystal structure of bHLH-DNA complex (PDB id: 4H10) (Wang et al., 2013) using UCSF-Chimera with bHLH domain perfectly coincide, and DNA in 4H10 was then added to the Epas1-Bmal1 complex.

For homology modeling with AlphaFold v2 (Jumper et al., 2021), amino acid sequence of pika Epas1 and Bmal1 bHLH-PAS domain (same with our ROSETTA model) was linked with a 40-poly-proline linker (Ko and Lee, 2021). The source code of AF2 was retrieved from the github repository (https://github.com/deepmind/alphafold) on July-16-2021. Template was allowed to use for structure modeling by setting the max_release_date parameter as 2021-07-29. The full_db preset was used for modeling. Ten models were generated, and the final model was rank_0 model.

Molecular dynamics modeling was performed to refine the complex model with GROMACS. Briefly, the simulation used amber14sb_parmbsc1 force field. The protein-DNA complex was placed in a cubic box with periodic boundary, which was filled with TIP3P water molecules and was neutralized with 150 mM NaCl solution. The system was energy minimized until the maximum force on any atom was less than 100 $kJ \cdot mol^{-1}nm^{-1}$, following equilibrated for 100 ps. A 300 ns molecular dynamics (MD) simulation was then completed. Protein-DNA complex was set in one temperature controlling group, and the environment set in another group.

For binding free energy calculation, we used MD refined structure of pika Clock-Bmal1 and Epas1-Bmal1 truncated PAS domain (to increase stability, relatively flexible bHLH domain was truncated) to perform umbrella sampling following the previous study (Lemkul and Bevan, 2010). Briefly, Clock or Epas1 was fixed and Bmal1 was pulled 10 nm (5 nm/ns, 2 ns) for generating configurations, and configurations in every 0.1 nm along the reaction axis were used as input for umbrella sampling.

Streptavidin affinity pull-down

The recombinant plasmid pET21a Strep tagged Epas1 was transformed alone or co-transformed with pET28a 6×His-SUMO tagged WT Bmal1 and mutant Bmal1 into BL21 *E.coli* cells respectively. Following the IPTG (100 μM) induced overnight expression at 16°C, cell pellets were lysed by sonication in a lysis buffer A. The Streptavidin beads were washed twice with lysis buffer A. After sonication and high-speed spinning, the cell lysate was loaded onto washed Streptavidin beads, then rotated for 2 h under room temperature. Streptavidin beads were washed with buffer A with rotation (4 min × 3 times). The elution samples were finally analyzed by Western blot.

ChIP-qPCR

Cell-based ChIP assays were performed following the protocol described previously (Wu et al., 2017). Briefly, unsynchronized and confluent pika/rat *Epas1* knock-in mouse fibroblast cells in 15 cm dishes were treated with 1 mM DMOG for 16h. After treatment, cells were cross-linked in DMEM containing 1 mM DMOG, PMSF, and 1% formaldehyde for 12 min at room temperature. The cross-link

was stopped by adding glycine to a final concentration of 125 mM and incubated at room temperature for 5 min. ChIP assay and DNA sample preparation were performed strictly following the ChIP-IT High Sensitivity Kit instructions (Active Motif). Eluted DNA was analyzed with high-throughput sequencing. For regular ChIP assays (FLAG-Epas1), 15 μg sheared mammalian chromatin and 4 μg Bmal1 or FLAG antibody were applied into a 200 μL reaction system, together with protease inhibitor cocktail. Throughout the whole process of ChIP, from sample fixing to IP, the reaction system was under 1 mM DMOG condition to avoid degradation of Epas1. The ChIP products were detected by qPCR to investigate the fold of enrichment. For primers, see Table S2.

LumiCycle recording of SCN

Pika or rat *Epas1* knock-in mice carrying *Per2-dLuc* were given pentobarbital sodium before euthanized by cervical dislocation at 8 weeks old. The brains were harvested quickly after death. Coronal sections (250 μm) were made using a vibrating microtome until the SCN is visible. The SCN was then transferred to Millicell culture plate inserts (PICMORG50, Millipore, Bedford, MA), cultured in explant media (DMEM supplement with 0.1 mM D-luciferin, pen/strep and 5% B27 supplement) and placed in LumiCycle (Actimetrics). After 3-4 days of recording, the SCN as well as the culture plate inserts were transferred to fresh explant media with 225 μM FG-4592 or 250 μM $NiCl_2$ before put back into the LumiCycle for another 3-4 days. The SCN and the culture plate inserts were then transferred to fresh explant media and recorded in LumiCycle for another 3-4 days.

Recombinant adeno-associated virus generation

The coding sequence of *Epas1* of pika or rat were cloned onto an AAV vector with V5 tag at the C-terminal. All AAV viruses were packaged into AAV serotype 9. The titers of the viruses ranged from 2 to 6 $\times 10^{10}$ viral particles per μL.

Stereotactic surgery and core body temperature recording

Before surgery, all mice were anesthetized with pentobarbital sodium. The mouse was fixed to the mouse brain locator, and the scalp was cut to expose the skull. AAV-pika *L-Epas1*-V5 or AAV-rat *Epas1*-V5 were injected with GFP expressing virus into the bilateral SCN (0.46 mm posterior and 0.25 mm lateral to the bregma, and 5.7 mm from the surface of the skull) of C57BL6 mice. 3 weeks later, E-mitter (Starr Life Sciences) was implanted into the mouse abdomen. Mice were allowed 1 week to recover before transferred to oxygen-controlled chambers and treated with 10% O_2 atmosphere with 12h:12h light/dark photoperiod for 3 days followed by 3 days in constant darkness.

Weight loss ratio

C57, Pika or rat *Epas1* knock-in mice were weighted before put in 10% O_2 atmosphere in an oxygen-controlled chamber for 1 month. All mice were then weighted again after one month. Weight loss ratio was determined as (weight of before-weight of after)/weight of before (Peng et al., 2017).

Hemoglobin detection

C57, pika or rat *Epas1* knock-in mice in chambers with hypoxia (10% O_2) or normaxia condition (21% O_2) for one month. All mice were anesthetized with pentobarbital sodium. Arterial blood samples were then collected from eyes for hemoglobin measurement. Hb concentration was determined using a spectrophotometer (Mission Hb, ACON).

HE staining

After one month of 10% O_2, C57, pika or rat *Epas1* knock-in mice were perfused with 4% paraformaldehyde in PBS under anesthesia. The hearts were quickly removed, and were fixed, dehydrated and embedded subsequently. 5 μm transverse slices from each heart were prepared for hematoxylin and eosin staining, and the images were acquired using Olympus VS120.

Assessment of right ventricular hypertrophy

C57, Pika or rat *Epas1* knock-in mice carrying Per2:LUC were weighted before put in 10% O_2 atmosphere in an oxygen-controlled chamber for 1 month. All mice were then weighted again before anesthetized with pentobarbital sodium. After perfusion with PBS, hearts of the mice were harvested, and the weight of the right ventricle and the combined weight of the left ventricle and the ventricle septum were analyzed. The ratio between the two was used to evaluate the level of right ventricular hypertrophy.

QUANTIFICATION AND STATISTICAL ANALYSIS

Statistical analysis for individual experiments is indicated as described in figure legends. Statistical significance was determined using a two-sided Student's t-test when only two groups were analyzed unless specifically noted. *$p < 0.05$, **$p < 0.01$, ***$p < 0.001$. GraphPad Prism and Excel were used for statistical analysis.